CHARACTERIZATION OF CURING KINETICS AND POLYMERIZATION SHRINKAGE IN CERAMIC-LOADED PHOTOCURABLE RESINS FOR LARGE AREA MASKLESS PHOTOPOLYMERIZATION (LAMP)

A Thesis
Presented to
The Academic Faculty

by

Kiran Kambly

In Partial Fulfillment
Of the Requirements for the Degree
Master of Science in Mechanical Engineering

Georgia Institute of Technology
Dec, 2009

CHARACTERIZATION OF CURING KINETICS AND POLYMERIZATION SHRINKAGE IN CERAMIC-LOADED PHOTOCURABLE RESINS FOR LARGE AREA MASKLESS PHOTOPOLYMERIZATION (LAMP)

Approved by:

Dr. Suman Das, Advisor
School of Mechanical Engineering
Georgia Institute of Technology

Dr. John Halloran
School of Materials Science and Engineering
University of Michigan

Dr. Kyriaki Kalaitzidou
School of Mechanical Engineering
Georgia Institute of Technology

Dr. Clifford. L. Henderson
Chemical and Biomolecular Engineering
Georgia Institute of Technology

Date Approved: Nov 10, 2009

For Shruti, who helped celebrate the leaps, mourn the falls, and gave me a good kick when I needed one.

ACKNOWLEDGEMENTS

It was on 30th June 2007, when I first got an opportunity to talk to Prof. Suman Das. From then on, it has been a tremendous learning curve in all aspects of my research mainly due to his dedicated passion for the success of his students. His vast pool of interdisciplinary knowledge is extremely commendable and the tireless efforts put in minuscule details, be it in discussing a concept or correcting a write-up is awe inspiring. His rock solid backing during my tough times has not only helped me to bounce back but has also driven my zest to continue further. Saying "I'm extremely grateful to him" would just be an understatement for the things that I have gained from this wonderful experience of having worked under his guidance. If not for his confidence over me, it may not have been possible for me to step into USA.

Darpa project members, Dr Dajun, Dr Rui, Peng, Anirudh, Dr.Vladka and Dr.Claudia played a crucial role in helping me design and conduct the experiments by maintaining extremely conducive work ambience. I sincerely thank them all and the rest of the group members for their cooperation. I'm extremely grateful to Paul, for his constant assistance on and off work during the entire course of my stay. I also take this opportunity to thank Dr. Satish Kumar , Dr. Haskel Beckham and their graduate students Yao dong and Ryan for permitting me to use their experimental apparatus. Finally, I thank my committee members, Prof John Halloran, Prof Kyriaki Kalaitzidou and Prof Clifford Henderson for readily agreeing to serve in my committee.

Lastly, I would like to thank my parents and my brother for their unconditional love and support in my every pursuit.

TABLE OF CONTENTS

	Page
ACKNOWLEDGEMENTS	iv
LIST OF TABLES	vii
LIST OF FIGURES	vii
LIST OF SYMBOLS AND ABBREVIATIONS	ix
SUMMARY	xi
CHAPTER	
1 INTRODUCTION	1
1.1 OPERATING PRINCIPLE OF LARGE AREA MASKLESS PHOTOPOLYMERIZATION	2
1.2 MOTIVATION AND OBJECTIVE	4
1.3 ORGANIZATION OF THESIS	6
2 LITERATURE REVIEW	8
2.1 EXPERIMENTAL SHRINKAGE CHARACTERIZATION	8
2.2 ANALYTICAL MODELS FOR SHRINKAGE	12
2.3 EXPERIMENTAL STRATEGIES FOR SHRINKAGE CONTROL	14
2.4 GAP ANALYSIS	17
2.5 SUMMARY	18
3 FUNDAMENTALS OF PHOTOPOLYMERIZATION SHRINKAGE	19
3.1 POLYMERIZATION KINETICS	19
3.2 SHRINKAGE STRAIN KINETICS	21
3.3 SHRINKAGE MEASUREMENT APPARATUS	23
3.3.1 Photo Differential Scanning Calorimetry (Photo-DSC)	23

3.3.2 Fourier Transform Infrared Spectroscopy (FTIR) 24
3.4 THEORETICAL RELATIONSHIP BETWEEN SHRINKAGE AND DEGREE OF CONVERSION 27
3.5 RESIN COMPOSITION AND PROPERTIES 29
3.5.1 Criteria for Selection of Photoinitiators 29
3.6 SUMMARY 32
4 RESULTS AND DISCUSSION 33
4.1 EFFECT OF VARYING PHOTOINITIATOR CONCENTRATION 34
4.1.1 Varying Irgacure (IR) 184 35
4.1.2 Varying Irgacure (IR) 819 38
4.2 EFFECT OF VARYING FILLER LOADING 41
4.3 RELATIVE VOLUMETRIC SHRINKAGE STRAIN 44
4.4 COMPARISONS BETWEEN IR 184 AND IR 819 53
4.5 PRINT-THROUGH MEDIATED INCREMENTAL CURING 55
4.6 SUMMARY 57
5 SUMMARY AND CONCLUSIONS 59
5.1 CONTRIBUTIONS 59
5.2 FUTURE WORK 60
REFERENCES 62

LIST OF TABLES

Page

Table 4.1: Experimental parameters. 34

LIST OF FIGURES

Page

Figure 1.1: Schematic illustration of Georgia Tech's LAMP machine. 3

Figure 1.2: Major functional tasks involved in DDM of airfoils using LAMP. 5

Figure 1.3: Organization of thesis. 7

Figure 2.1: Schematic cross-section of the shrinkage test assembly. 10

Figure 3.1: Schematic of the photopolymerization process. 19

Figure 3.2: Polymerization rate as a function of irradiation time. 22

Figure 3.3: FTIR operated in attenuated total reflectance (ATR) mode. 25

Figure 3.4: FTIR spectrum of acrylate monomer undergoing photopolymerization. 27

Figure 3.5: Spectrum of high pressure mercury vapor lamp. 31

Figure 3.6: Absorption spectrum of IR 184. 31

Figure 3.7: Absorption spectrum of IR 819. 32

Figure 4.1: Conversion vs. energy dose for varying concentration (wt %) of IR 184. 36

Figure 4.2: Rate of polymerization vs. conversion for varying concentration (wt %) of IR 184. 37

Figure 4.3: Dependence of R_{pmax} on the fraction of absorbed energy for varying concentration (wt %) of IR 184. 37

Figure 4.4: Conversion vs. concentration (wt %) of IR 184 for the fastest exposure

time on LAMP machine. 38

Figure 4.5: Conversion vs. energy dose for varying concentration (wt %) of IR 819. 39

Figure 4.6: Rate of polymerization vs. conversion for varying concentration (wt %) of IR 819. 40

Figure 4.7: Conversion vs. concentration (wt %) of IR 819 for fastest exposure time on LAMP machine. 40

Figure 4.8: Dependence of R_{pmax} on the fraction of absorbed energy for varying concentration (wt %) of IR 819. 41

Figure 4.9: Conversion vs. energy dose for varying filler loading (vol %). 42

Figure 4.10: Rate of polymerization vs. conversion for varying filler loading (vol %). 43

Figure 4.11: Rate of polymerization vs. energy dose for varying filler loading (vol %).43

Figure 4.12: Conversion vs. filler loading (vol %) at a constant exposure time of 60ms (0.984kJ/m^2). 44

Figure 4.13: Three-dimensional plot of volumetric shrinkage strain as a function of energy dose and degree of conversion for varying concentration (wt %) of IR 184. 46

Figure 4.14: Volumetric shrinkage strain vs. energy dose for photocurable material system with 60% filler loading and photoinitiator IR 184. 47

Figure 4.15: Volumetric shrinkage strain vs. degree of conversion for photocurable material system with 60% filler loading and photoinitiator IR 184. 47

Figure 4.16: Three-dimensional plot of volumetric shrinkage strain as a function of energy dose and degree of conversion for varying concentration (wt %) of IR 819. 49

Figure 4.17: Volumetric shrinkage strain vs. energy dose for photocurable material system with 60% filler loading and photoinitiator IR 819. 49

Figure 4.18: Volumetric shrinkage strain vs. degree of conversion for photocurable material system with 60% filler loading and photoinitiator IR 819. 50

Figure 4.19: Three-dimensional plot of volumetric shrinkage strain as a function of filler loading (vol%) and degree of conversion for varying energy dose and 0.43% of IR 184. 51

Figure 4.20: Volumetric shrinkage strain vs. degree of conversion for photocurable material system with 0.43% IR 184, varying filler loading (vol %) and energy dose. 52

Figure 4.21: Shrinkage strain vs. conversion for IR 184 and IR 819. 54

Figure 4.22: Shrinkage strain vs. exposure time for IR 184 and IR 819. 55

Figure 4.23: Print-through mediated incremental curing at the bottom layer due to exposures of layers above it. 56

Figure 4.24: Conversion in the bottom layer vs. number of exposures above the bottom layer. 57

LIST OF SYMBOLS AND ABBREVIATIONS

A	Absorbance of the sample
d	sample thickness, m
f_i	Functionality of the monomer i
I_{abs}	Intensity of absorbed radiation in the sample
I_0	Incident intensity of radiation
ΔH_p	Enthalpy of polymerization (kJ/kg)
k_p	Rate constant of propagation
k_t	Rate constant of termination
[M]	Monomer mixture concentration (wt %)
M_m	Molecular weight of the monomer (mol/g)
m	Mass of the pure monomer (kg)
[PI]	Photoinitiator concentration (wt %)
R_p	Rate of polymerization (mol/l/s)
R_{p_max}	Maximum rate of polymerization (mol/l/s)
V	Volume (m^3)
$\Delta V/V$	Volumetric shrinkage strain (%)

Greek symbols

α	Degree of conversion (%)
ε	Molar extinction coefficient (l/cm/mol)
ρ_m	Density of the monomer (kg/m^3)
ρ_{mix}	Density of monomer mixture (kg/m^3)
χ_i	Mole fraction of monomer i
φ_i	Initiation quantum yield

Abbreviations

LAMP	Large Area Maskless Photopolymerization
DDM	Direct Digital Manufacturing
DMD	Digital Micromirror Device
SLA	Spatial Light Modulator
FTIR	Fourier Transform Infrared Spectroscopy
DSC	Differential Scanning Calorimetry
HDDA	Hexanediol Diacrylate
EPETA	Ethoxylated Penta-erithrytol Tetraacrylate
IR 184	Irgacure 184, photoinitiator supplied by CIBA
IR 819	Irgacure 819, photoinitiator supplied by CIBA

SUMMARY

Large Area Maskless Photopolymerization (LAMP) is a direct digital manufacturing technology being developed at Georgia Tech to produce ceramic molds for investment casting of turbine airfoils. In LAMP, UV light incident on a spatial light modulator is projected in the form of a structured black and white bitmap image onto a platform supporting slurry comprising a ceramic particle loaded photocurable resin. Curing of the resin is completed rapidly with exposures lasting 20~160ms. Three-dimensional parts are built layer-by-layer by sequentially applying and selectively curing resin layers of 25-100 micron thickness. In LAMP, diacrylate-based ceramic particle-loaded resins with photoinitiators sensitive in the range of spectral characteristics of the UV source form the basis for an ultra-fast photopolymerization reaction. At the start of the reaction, the monomer molecules are separated by van der Waals distance (~10^4Å). As the reaction proceeds, these monomer molecules form a closely packed network thereby reducing their separation to covalent bond lengths (~ 1 Å). This results in bulk contraction in the cured resin, which accumulates as the part is fabricated layer-by-layer. The degree of shrinkage is a direct measure of the number of covalent bonds formed. Thus, shrinkage in LAMP is characterized by estimating the number of covalent bonds formed during the photopolymerization reaction.

Polymerization shrinkage and accompanying stresses developed during photopolymerization of ceramic particle-loaded resins in LAMP can cause deviations from the desired geometry. The extent of deviations depends on the photoinitiator concentration, the filler loading, the degree of monomer conversion, and the operating

parameters such as energy dose. An understanding of shrinkage and stresses built up in a part can assist in developing source geometry compensation algorithms and exposure strategies to alleviate these effects. In this thesis, an attempt has been made to understand the curing kinetics of the reaction and its relation to the polymerization shrinkage. Real-time Fourier Transform Infrared Spectroscopy (RTFTIR) is used to determine the conversion of monomers into polymer networks by analyzing the changes in the chemical bonds of the participating species of molecules. The conversion data can further be used to estimate the curing kinetics of the reaction and the relative volumetric shrinkage strain due to polymerization.

CHAPTER 1
INTRODUCTION

Large Area Maskless Photopolymerization (LAMP) is a direct digital manufacturing (DDM) technology which combines layered manufacturing of complex three-dimensional objects by solid freeform fabrication with the fine-feature resolution and high throughput of massively parallel scanning maskless lithography to achieve a disruptive breakthrough in part build speed and feature resolution. The maskless lithography system in LAMP comprises of a spatial light modulator (SLM) which is a digital micro-mirror device (DMD) chip developed by Texas Instruments. It is an optical chip with more than 1.3 million tiny mirrors that can be turned on or off selectively according to the pixels in a corresponding black and white bitmap image. Light from a UV source strikes the DMD chip and the various mirrors turn on and off accordingly to project the input image on to the surface of a photocurable ceramic-loaded liquid resin. The optical imaging head, consisting of the UV source and the DMD chip, raster scans the entire exposure region in a serpentine path. This exposure mechanism results in much higher patterning speeds than conventional stereolithography processes in which a single laser beam is used to raster scan the exposure region line by line. In addition, due to the high scanning speeds (~400mm/s), extremely large areas (of the order 750cm^2) can be patterned without compromising feature resolution (~20μm).

Currently, turbine airfoils with extremely complex interior cooling passages are produced by investment casting. The process begins with the creation of all the tooling necessary to fabricate the cores, patterns, mold, and setters for casting airfoils, typically involving over thousand tools for each airfoil [1]. The subsequent steps involve ceramic

core fabrication by injection molding. Molten wax is also injection molded to define the patterns for the airfoil shape. Several such wax patterns are then subjected to multiple rounds of slurry coating to form completed mold assembly. The mold assembly is then placed in an autoclave for dewaxing resulting in a hollow ceramic shell mold into which molten metal is poured to form castings. Upon solidification, the ceramic mold is broken away and the individual metal castings are separated.

DDM of airfoils using LAMP will directly produce integral ceramic cored molds ready for casting as such eliminating over 1000 tools and all the above discussed conventional process of investment casting thereby making the lost wax process obsolete and dramatically improving casting yield, production time and associated costs. Thus, DDM using LAMP is a concept that disrupts the current state-of-the-art investment casting process for wide ranging applications. It opens new possibilities for designing and manufacturing components which would otherwise be difficult or impossible to manufacture conventionally.

1.1 Operating Principle of LAMP

A schematic of the LAMP process being designed and developed by the direct digital manufacturing (DDM) laboratory at Georgia tech is shown in figure 1.1. First, a 100μm thick layer of a UV-curable ceramic-filled resin is applied on the build platform. UV light reflected from the mirror is directed on to a spatial light modulator which is carried by a maskless optical imaging system that scans the build area in a serpentine path at high speeds projecting high resolution bitmap patterns on to the resin. The resin is cured and solidified into the desired patterns and the material platform moves down by

the build layer thickness of 100 μm. A new layer of resin is applied by the material recoating system and the process is continued until all the layers are built. The three-dimensional object is then retrieved from the build platform by draining the excess liquid resin and washing the uncured resin using solvents such as isopropanol and denatured alcohol. The as-cured object is then subjected to binder burnout and furnace sintering processes to remove the polymer without damaging the object and further densify the ceramic body to 60-80% relative density.

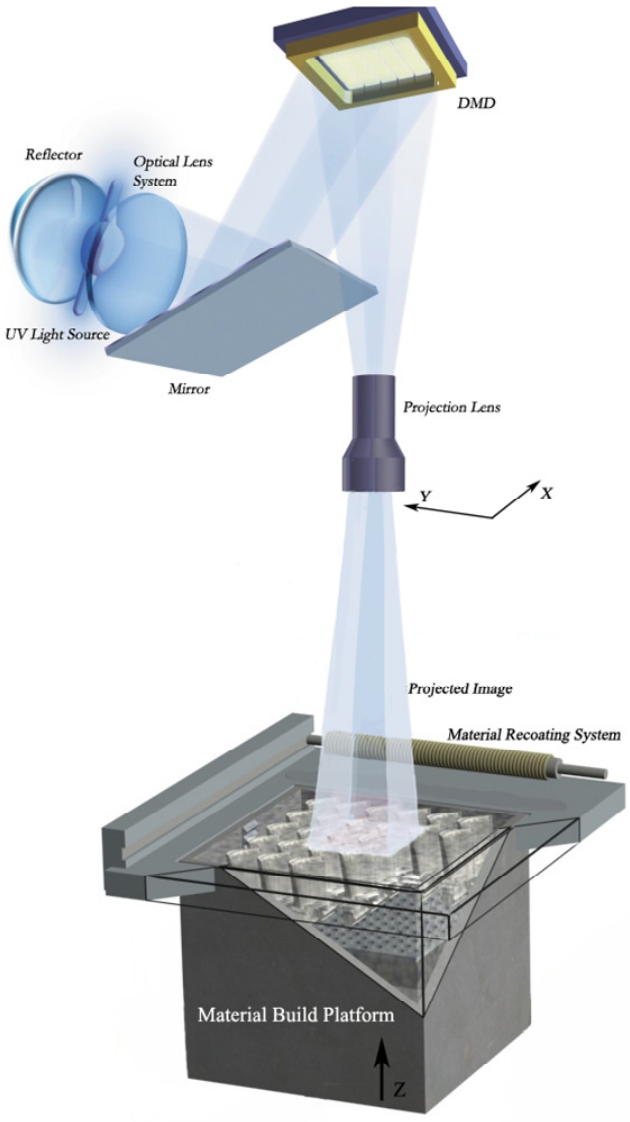

Figure 1.1 Schematic illustration of Georgia Tech's LAMP machine.

1.2 Motivation and Objective

The development of a direct digital manufacturing (DDM) technology based on LAMP involves several tasks requiring fundamental investigations. Some of the associated major tasks are shown in figure 1.2. All the tasks are inter-related and inputs from these are essential for the overall development of the LAMP process. To start with, the first stage in fabricating a three-dimensional part requires patterns of the slice cross-sections at 1500 dpi in order to maintain feature resolutions of 16~17μm. This task requires developing high frame rate data transport algorithms and softwares to transform the CAD slice data into a stack of bitmap images. Design and development of the LAMP machine also involves complete machine design including design of a material recoating system, a material build platform, a maskless optical imaging system and related automation, along with synchronization of these subsystems. The development of a photocurable material system involves cure depth investigations and resin sensitivity studies that are important for process development. Modeling of the LAMP process to simulate photopolymerization kinetics will assist in quickly determining shrinkage without the need for additional experiments. The post-cure shrinkage and stress analysis after binder burnout process by firing and sintering plays an important role in controlling the quality of the metal casting. The focus of the present work is that, the cured area is observed to deviate from the original area of the pattern. The overall cumulative variation leads to a disparity between the design and the actual dimensions of a three-dimensional part along with internal stress build up. The photopolymerization reaction results in contraction in the layers during the complex formation of polymer networks between monomer molecules. The rate of contraction due to photopolymerization reaction is a

function of several mixture constituents such as the photoinitiator concentration, ceramic filler content, exposure energy dose and the degree of monomer conversion. The objective of this study is to systematically study the curing kinetics and to understand its effect on photopolymerization shrinkage. This study is motivated by the need to control photopolymerization shrinkage and related stresses that can cause part distortion during the LAMP process resulting in cracks, delamination and loss of geometric accuracy.

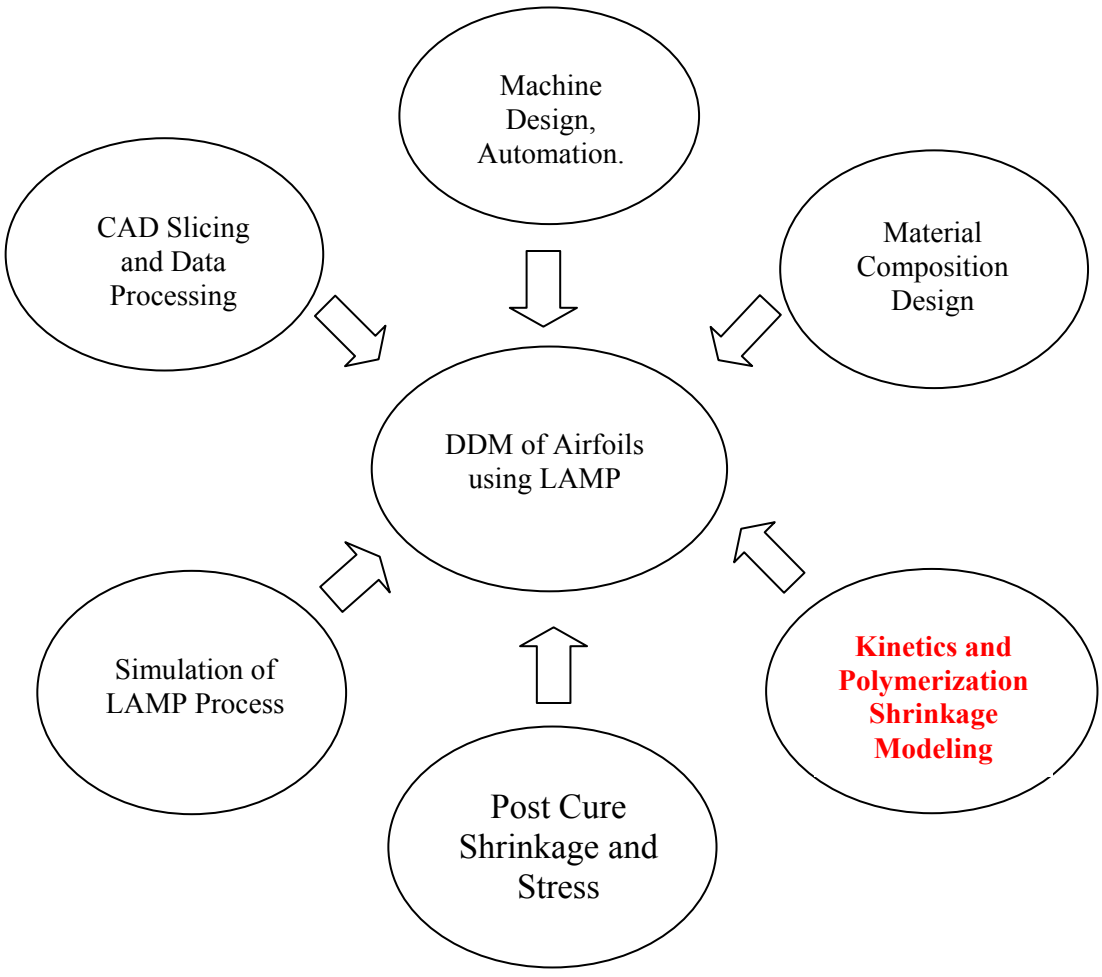

Figure 1.2 Major functional tasks involved in DDM of airfoils using LAMP.

1.3 Organization of Thesis

Figure 1.3 provides an overview of this thesis. Chapter 2 comprises of a literature review on several prominent works pertinent to this research. This chapter is divided into three major sections. In the first section, experimental characterization of curing kinetics using shrinkage measurement apparatus such as photo-DSC, water dilatometer and bonded disk measurement apparatus are reported. In the second section, analytical studies of curing kinetics and photopolymerization shrinkage for pure monomer systems are reported. Research related to several novel exposure strategies to minimize shrinkage is discussed in the last section. This chapter closes with gap analysis to avoid any overlap and to identify shortcomings from previous works. It establishes the potential for advancing our understanding of curing kinetics and shrinkage measurements in the LAMP process. Chapter 3 briefly introduces reaction mechanisms during photopolymerization. Shrinkage characterization using photo-DSC and FTIR spectroscopy are described in detail. The relationship between shrinkage and the degree of conversion is discussed and their relation with several key parameters such as photoinitiator concentration, filler loading in the resin compositions, and energy dose is investigated. The chapter concludes with details on resin preparation and criteria for selecting appropriate photoinitiators for the LAMP process. Chapter 4 details the experimental results of curing kinetics in terms of degree of conversion and rate of polymerization for a photocurable material system involving two different photoinitiator species. Similar analysis is performed and the results are presented for varying filler loading in the resin composition with a fixed photoinitiator concentration. Further, these results are used to determine shrinkage strain due to photopolymerization from the

relations described in chapter 3. The last section of chapter 4 presents results on change in the degree of conversion in the first layer due to multiple exposures from layers above. This leads to an understanding of penetrative effects of the UV source for a given composition and hence assists in tuning the resin composition to avoid problems such as print-through and side-scattering. The final chapter draws conclusions from the results presented in the previous chapter with a summary of contributions. The limitations of the present work are identified and areas for further improvements are suggested.

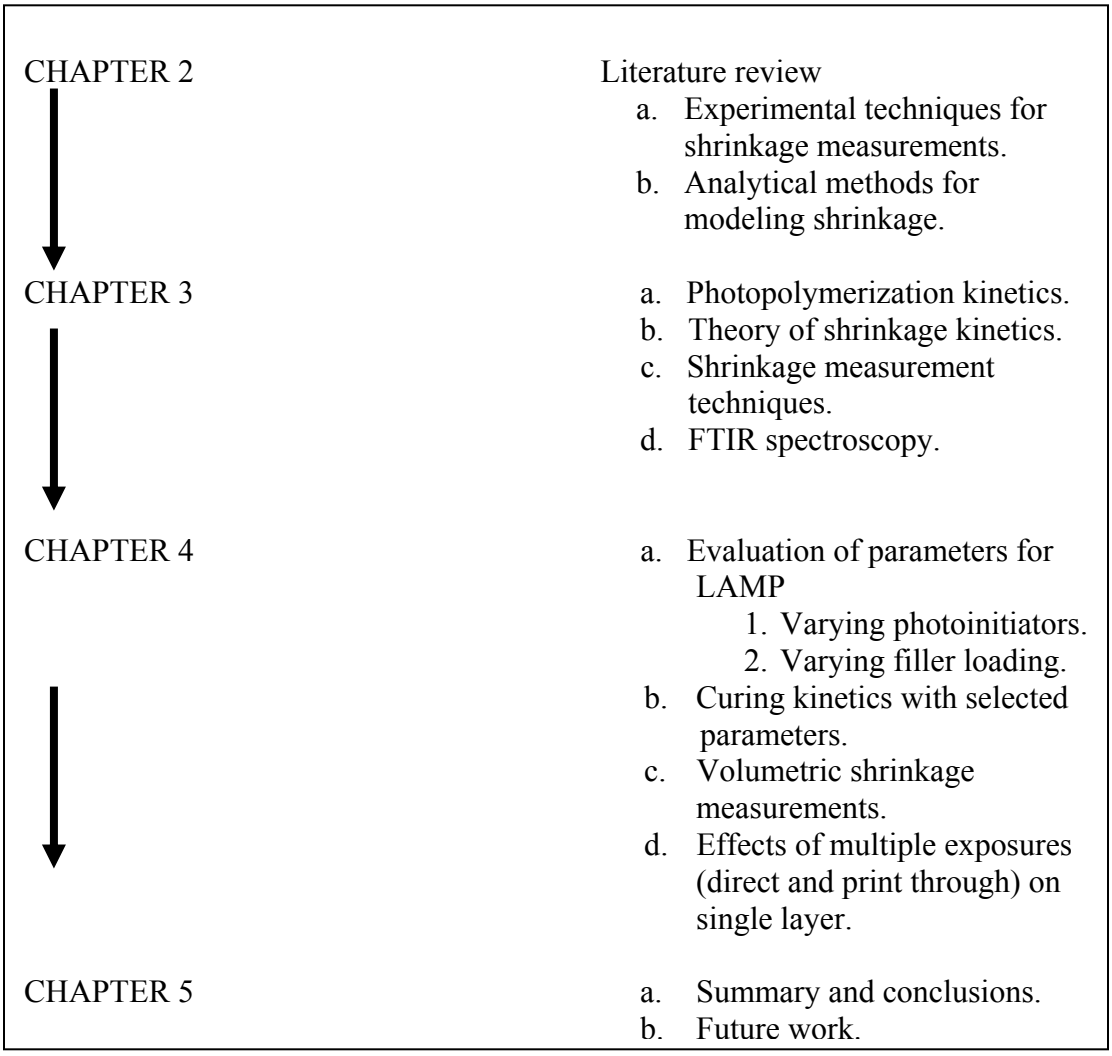

Figure 1.3 Organization of thesis.

CHAPTER 2
LITERATURE REVIEW

In this section, prominent results from the literature associated with the studies of curing kinetics and photopolymerization is discussed. Due to the complicated nature of reaction mechanisms during photopolymerization coupled with the advent of new monomers and photoinitiating species, the quest for fundamental understanding of curing kinetics has led to regular contributions in this field. Due to the existence of vast number of monomer systems, studies related to acrylate monomers are chosen here, since LAMP is carried out with ceramic-loaded multiacrylate monomers. This chapter is further divided into sections discussing experimental techniques using bonded disk measurement apparatus, near infrared spectroscopy, stray-field magnetic resonance imaging, electron spin resonance, analytical modeling and optimization strategies for determining curing kinetics and volumetric shrinkage with specific focus on compositions with filler contents.

2.1 Experimental Shrinkage Characterization

Atai and Watts [2] studied the effect of filler content on the shrinkage-strain kinetics and degree of conversion of composites. A resin matrix containing 65 wt. % bisphenol A glycidyl methacrylate (Bis-GMA) and 35 wt. % triethyleneglycol-dimethacrylate (TEGDMA) was prepared. Camphorquinone and dimethyl aminoethyl methacrylate with (0.5 wt %) each were dissolved in the resin as photoinitiators. Silanized glass fillers were added in different percentages to the resin-monomers. The shrinkage-strain in specimen's photopolymerized with energy dose of 550 mW/cm^2 was

measured using the bonded disk technique at 23°C, 37°C and 45°C for the matrix monomers and at 23°C for the composites. Initial shrinkage-strain rates were obtained by numerical differentiation of shrinkage-strain data with respect to time. It was also concluded that the surface area of the filler affects the degree of conversion of the composites more than the filler fraction.

Watts [3] attempted to develop a relationship between photocuring composites and the polymer-network forming reactions, along with their kinetics, and the resultant stress-transmitting micro-mechanical behavior. Expressions for light irradiance as a function of depth within materials were computed and the consequences of steady-state assumptions in kinetic models of conversion and shrinkage-strain rate were addressed. The resultant stress-transmitting properties were shown as a complex function of photon-transport, absorption by photoinitiators, possibly non-steady-state free-radical cross-linking, collapse of free-volume and development of an elastic-network displaying non-homogenous structure, viscoelasticity, and aging effects.

Watts and Hindi [4] prepared a resin-composite based on multi-acrylate monomers to evaluate differences in the setting shrinkage-strain kinetics relative to more conventional formulations based on dimethacrylate monomers. Four resin-composites were examined for shrinkage-strain over time periods up to 60 min, from initial irradiation, using a 'bonded disk' measurement device. Reductions in the rate of initial shrinkage and in the final equilibrium shrinkage-strain were suggested to be achieved either by special light irradiation regimes (low to high or ramped) or in favorable cases by novel monomer-composite formulations and setting chemistry.

Watts and Cash [5] developed an instrument known as 'bonded disk apparatus', shown in Figure 2.1, for the reproducible measurement of polymerization shrinkage kinetics. The instrument is constructed around a disc-shaped specimen sandwiched between two glass plates. Test specimens of light-activated resins were irradiated through the lower, rigid plate. The upper non-rigid plate was readily deflected by an increase of the adhesive stress from the polymerizing and shrinking sample. Deflection was measured by a linear variable differential transducer (LVDT) and recorded. Shrinkage data was reported for representative unfilled and composite resins. Equilibrium shrinkage magnitudes ranged from 1.3 to 7.9%.

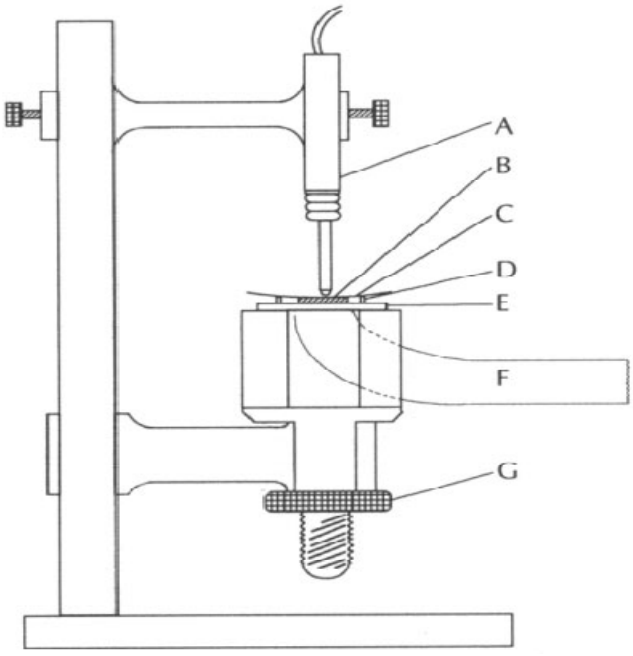

Figure 2.1 Schematic cross-section of the shrinkage test assembly: (A). LVDT transducer, total length 90 mm; (B). test specimen, diameter 8 mm; (C). flexible diaphragm, thickness 0.13 mm; (D). support ring, internal diameter 16 mm, height 1.5 mm; (E). rigid glass or quartz plate; (F). fibre-optic light guide, exit diameter 8 mm; (G). height adjustment screw [5].

Gao and Nie [6] studied the solid-state system of 1, 6-hexanediol diacrylate (HDDA)/2-hydroxyl-2-methyl-1-phenyl-propane-1-one (1173). Equipments such as near-infrared spectroscopy (NIR) and electron spin resonance (ESR) were employed to monitor the photopolymerization kinetics and the post-curing reaction of this system. Although the solid-state 1, 6-hexanediol diacrylate could be photoinitiated by 1173, the double bond conversion was observed to be low. The post-curing reaction was suggested to improve the double bond conversion. The photopolymerization kinetics were observed to be greatly affected by polymerization temperature. Increasing the curing temperatures caused an increase in the double bond conversion. The optimum concentration of 1173 was 0.4% for reaching high rate of polymerization and double bond conversion. However, excessive photoinitiator was found to decrease the rate of polymerization and double bond conversion.

Alvarez-Gayosso et al [7] calculated the contraction rate that results from polymerization shrinkage in fourteen different photocured resins using bonded disk method. Six measurements were made on each material at 20±2°C and 70±10% RH. Means and standard deviations were analyzed. Total shrinkage strain for photopolymerized resins (packable and flowable composites) varied between 1.65 and 4.16%. The contraction rate for photopolymerized resins varies between 55.71 and 167.00 μm/min. Packable resins presented a lower contraction rate than flowable resins. The monomer percentage affected the contraction rate, because higher contraction rate implies higher percentage of monomer. It was also inferred that contraction rate bears some relation to polymerization shrinkage.

Wu et al [8] studied the curing kinetics of UV-curable acrylate monomer-based ceramic resins using FTIR spectroscopy with an internally-mounted UV curing source, providing real-time quantification of the acrylate double bond conversion with respect to increasing UV dose. Real-time FTIR was found to provide a simple but valuable means of investigating average photopolymerization kinetics and final conversion in a thin layer of highly loaded ceramic suspension. Complete agreements of FTIR technique with photo differential scanning calorimetry (photo-DSC) experiments were shown. FTIR was also used to investigate the curing behavior inside sublayers of the same ceramic suspension. Curing kinetics and final conversion were monitored in these layers, with higher conversion and faster kinetics being observed near the exposed surface. Due to the scattering and absorption effects within the uppermost layers, photopolymerization rate and percent conversion declined as a function of depth from the surface.

2.2 Analytical Models for Shrinkage

Atai and Watts [2] developed a new kinetic model for the shrinkage-strain rates of dental resin composites. The degree of conversion in composites containing different filler contents was measured using FTIR spectroscopy. The model was developed for the shrinkage-strain rate using the autocatalytic model which is used to describe the reaction kinetics of thermoset resins. The model predictions were in good agreement with the experimental data. The results also showed a linear correlation between the shrinkage-strain (and shrinkage-strain rate) and filler-volume fraction. The filler fraction did not affect the degree of conversion of the composites. The rate of polymerization was determined via the shrinkage and was invariant with filler-fraction, suggesting that only a

relatively high filler-surface area, as may be obtained with nano-fillers, will affect the network-forming kinetics of the resin matrix.

Petrovic and Atanackovic [9] formulated an analytical model for the shrinkage strain developed during photopolymerization on the basis of a general procedure described to solve a fractional order differential equation [10]. The model is based on the diffusion type fractional order equation, since it has been proven that polymerization reaction is diffusion controlled [2]. This model also confirms the similar experimental observations by Atai and Watts [11]. The shrinkage strain is modeled by a nonlinear differential equation and is solved numerically. A linear fractional order differential equation was used to describe the strain rate due to photopolymerization. This equation is solved exactly. As shrinkage is a consequence of the polymerization reaction and polymerization reaction is diffusion controlled, this led to the postulate that shrinkage strain rate can be described by a diffusion type equation. An explicit form of the solution to this equation determines the strain in the resin monomers. Stresses in the polymer due to the shrinkage were determined by using equations of linear viscoelasticity. The time evolution of stresses implied that the maximal stresses are developed at the very beginning of the polymerization process. The stress in a composite that is light treated has the largest value a short time after the treatment starts. The strain settles at a constant value in the timescale of about 100 s (for the cases treated in [11]). The shrinkage strain of composites and resin monomers was analytically determined. The maximum stress determined here depends on the diffusivity coefficient. Since the diffusivity coefficient increases as polymerization proceeds, it follows that the periods of light treatments should be shorter at the beginning of the treatment and longer at the end of the treatment,

with dark interval between the initial low intensity and following high intensity curing. This is due to the inability of stress relaxation to occur at the end of polymerization.

Scherzer [12-13] used time-resolved FTIR-ATR spectroscopy to study the kinetics of photopolymerization of a diacrylate using a morpholino ketone as the photoinitiator. The curing reaction was induced by monochromatic UV radiation with a wavelength of 313 nm. The influence of photoinitiator concentration [PI], light intensity I_0, temperature, and monomer functionality on kinetic parameters like polymerization rate Rp, induction period, and the double bond conversion was investigated. The dependence of Rp on [PI] and I_0, was found to fit with theoretical predictions very well. In contrast, an increase in the temperature was found to have no effect on Rp. various photoinitiator systems were tested for their efficiency to start the curing reaction of acrylates on irradiation with light of wavelength 313 nm or 222 nm. The contribution of postcuring to the final conversion was determined by following the decay of the double bonds during and after irradiation with single or multiple short UV flashes with duration of 50-200 ms.

2.3 Experimental Strategies for Shrinkage Control

Lu et al. [14] showed that low volumetric shrinkage of poly-triethylene glycol dimethacrylate was made possible by photopolymerization at a low temperature. The final double-bond conversion and dynamic mechanical analysis indicated the optimal cure temperature to be 40°C, at which a cured sample had less volumetric shrinkage than samples cured at room temperature but with similar mechanical properties.

Chung et al. [15] evaluated the potential of a novel trifunctional methacrylate as a component of a photocurable composite resin with reduced curing shrinkage. Tris[4-(2

prime -hydroxy-3 prime - methacryloyloxypropoxy)phenyl]methane (TTEMA) was synthesized by reacting triphenylolmethane triglycidyl ether (TTE) with methacrylic acid in the presence of 4-(dimethylamino) pyridine. Photopolymerization reactivity and volumetric shrinkage of unfilled resins based on TTEMA were investigated by FTIR and density measurements, respectively, and the results were compared with those for conventional monomers. A three-point bending test of the TTEMA-containing composite resin was carried out. Unfilled resins of TTEMA and bis-GMA, each containing 40% TEGDMA, showed similar photopolymerization reactivity. TTEMA exhibited very low photopolymerization shrinkage of 2.09%, and 3:2 TTEMA-TEGDMA unfilled resins revealed 10% lower shrinkage than a conventional bis-GMA system containing the same amount of TEGDMA. The flexural strength of a light-activated composite resin formulated with TTEMA is comparable to that of a bis-GMA composite resin under the same conditions. TTEMA was found promising for application as a photocurable monomer due to ease of synthesis, good polymerization reactivity, and relatively low curing shrinkage.

Khudyakov et al [16] discussed several strategies for shrinkage control. It has been shown that high intensity lights provide higher values for degrees of conversion and physical properties although they also produce higher contraction strain rates during composite polymerization. A slower curing process has been shown to allow stress relaxation to take place during the polymerization process. An approach was designed to allow the resin composite some freedom of movement consisting of an initially reduced conversion degree of the resin material. The application of a lower intensity light for a longer period time or use of variable intensities over a given period time was suggested.

These techniques initially use low-intensity curing for a short period of time in order to provide sufficient network formation on the composite surface while delaying the gel point in the lower layers until a final high-intensity polymerization is initiated. However, several other authors [17-18] did not find any improvement using this 'soft-start polymerization' method due to different concentrations of photoinitiators. This led to the conclusion that certain resin-based composites required shorter exposure time to achieve the same degree of conversion while maintaining the intensity constant.

Pereira [19] performed in-situ monitoring of photopolymerization of four dimethacrylate monomers under different irradiation conditions by 1H stray-field magnetic resonance imaging (1H STRAFI-MRI). This technique was found to be capable of discriminating local changes at a spatial resolution of tens of microns and suitable for studying larger samples than those possible with infrared spectroscopy and photocalorimetry. The evolution of proton magnetization with irradiation time and intensity was recorded and correlated with volumetric polymerization shrinkage, extent of reaction, and spatially resolved reaction rates.

Condon and Ferracane [20], worked on composites which included nanofiller particles that were not treated with a functional agent and coupled them to the resin matrix. It was observed that this procedure resulted in lower stress levels. Three types of nanofillers were evaluated having either a functional silane coating, a non-functional silane coating, or no coating. These were added at five different loading levels by volume to a photopolymerizable mixture of three dimethacrylate monomers alone or at three different volume loading levels to the same resin filled with filler particles. The stress generated by these materials when cured in a confined setting was measured in a

mechanical testing machine. The effect of monomer molecular weight on the stress levels was evaluated by preparing three resin formulations with varied co-monomer levels and filling them with bonded or non-bonded nanofillers. Reductions in polymerization stress of up to 31% were achieved among the nanofilled resin composite. The materials which contained a heightened level of diluent monomer produced significantly higher stress levels leading to a conclusion that major reductions in polymerization stress can be achieved through minor alterations in composite chemistry.

2.4 Gap Analysis

From the above literature survey, it can be seen that photopolymerization kinetics and contraction rates have been studied extensively for several pure monomers except in [8, 11] where filler particles were present in the reaction mixture. In the research involving monomer mixtures with fillers, the curing process involved single line exposures using UV light pens unlike in LAMP. This necessitates the need to estimate the curing kinetics and shrinkage strains for resins with filler content processed through LAMP, which involves layer by layer curing. Further, results from this research are also intended to augment the process evaluation for a wide range of operating conditions based on the resin composition and properties with the objective of minimizing the shrinkage strain on parts fabricated with LAMP.

2.5 Summary

This chapter provided a summary of previous work relating to photopolymerization of pure monomer systems and of composite systems. Several different analysis methods were presented ranging from purely experimental procedures to analytical expressions complimenting the former. Distinct properties of the participating species in terms of their chemical structures, reacting potentials and curing techniques does not permit broad generalization of the application of any individual technique for evaluating curing kinetics and optimizing contraction rates. Hence it is important to know the merits and range of applicability of these techniques on a case by case basis. In a dynamic layer-by-layer manufacturing process like LAMP, it is important to choose a technique which would permit quick and accurate estimation of curing kinetics and shrinkage strain measurements without the need for extensive additional instrumentation and processing time. The research gap discussed in the previous section establishes the need to further advance the shrinkage strain analysis for LAMP.

CHAPTER 3

FUNDAMENTALS OF PHOTOPOLYMERIZATION SHRINKAGE

In this chapter, the fundamentals of photopolymerization kinetics at various stages of the polymerization reaction are discussed. Several experimental techniques to quantify the shrinkage during photopolymerization are studied in detail to evaluate their ease of applicability for LAMP. Preparing the right type of material composition is critical to LAMP process and hence is worth discussing the necessary requirements.

3.1 Photopolymerization Kinetics

A comprehensive photopolymerization model is developed by Goodner and Bowman [21], based on the three primary reaction mechanisms occurring during the polymerization: initiation, propagation, and termination (figure 3.1). The model also incorporates both primary radical termination and inhibition.

Initiation

$$I \xrightarrow{h\upsilon} 2R\bullet \quad (3.1)$$

$$R\bullet + M \xrightarrow{k_i} P_1\bullet \quad (3.2)$$

$$P_n Z\bullet + M \xrightarrow{k_i'} P_{n+1}\bullet \quad (3.3)$$

Propagation

$$P_n\bullet + M \xrightarrow{k_p} P_{n+1}\bullet, \quad (3.4)$$

Termination

$$P_n\bullet + P_m\bullet \xrightarrow{k_t} P_{n+m}/P_n + P_m \quad (3.5)$$

$$P_n\bullet + R\bullet \xrightarrow{k_{tp}} P_n \quad (3.6)$$

Inhibition

$$P_n\bullet + Z \xrightarrow{k_z} P_n Z\bullet. \quad (3.7)$$

Figure 3.1 Schematic of the photopolymerization process [21].

In the reaction mechanism shown in figure 3.1, Eq. 3.1 is the photolysis of initiator, I, to give two primary radicals, R•. The second step of initiation is the chain initiation process, represented by Eq. 3.2. In this reaction, a primary radical reacts with the monomer, M, to form a growing polymer chain one repeat unit in length, P_1•. The rate of this reaction is determined by the kinetic constant for chain initiation, k_i. A second type of chain initiation is given by Eq. 3.3 which is re-initiation of inhibited chains. In this reaction, an inhibited chain, P_nZ•, reacts with the monomer to form actively growing chain. The kinetic constant for reinitiation, k_i' will in general be different from k_i; in fact, the value of k_i', in most systems is either considerably lower (several to many orders of magnitude) than k_i or is considered to be zero. The propagation reaction is represented by a single reaction (Eq. 3.4), and the kinetic constant for propagation is k_p.

Chain termination occurs through two different mechanisms. Bimolecular termination (Eq. 3.5) occurs when two growing radical chains come together and react to form dead polymer; this reaction can either occur by combination (forming one polymer chain) or disproportionation (forming two chains). While the mode of termination significantly affects the molecular weight in linear polymer-forming systems, the polymerization kinetics in cross-linked systems, which are predominant in commercial photopolymer applications, are not influenced significantly by the termination mode. Thus, the bimolecular termination reaction will be lumped into a single reaction having kinetic constant k_t. The second termination mechanism is primary radical termination (Eq. 3.6), in which a primary radical reacts with a growing polymer chain to form dead polymer. The kinetic constant for this process, k_{tp}, will in general be different from the bimolecular termination rate constant k_t, as the two reactions have different chemistry

and different species mobilities involved in the termination process. The last reaction occurring during polymerization is chain inhibition (Eq. 3.7). In this process, an inhibitor species, Z, such as molecular oxygen or an intentionally added inhibitor, reacts with a growing chain to form a relatively unreactive species. The kinetic constant for this reaction is k_z.

3.2 Shrinkage Strain Kinetics

Polymerization shrinkage in UV-curable composites is the result of a change in the intermolecular distances of the resin-monomers which are initially at van der Waals length scales (~10^4 Å) to the covalent bond lengths (~1 Å) during photopolymerization [22]. As shrinkage is a consequence of the polymerization reaction, it should follow the polymerization reaction pattern. The polymerization rate exhibited by the monomers during curing process is illustrated in figure 3.2. The rising part at the early stage of the reaction and falling parts of the polymerization rate, represent the auto-acceleration and auto-deceleration stages of the polymerization reaction respectively. The auto-acceleration effect reaches a maximum which is referred to as the "gel point". The gel point is that stage of the reaction where a loose network of polymer is formed and significant change is the viscosity is observed. However the monomers are still not locked in their position requiring more curing time to form a complete solid network. This trend is seen in the polymerization of diacrylate monomers [16, 23]. Photopolymerization and network formation of the multifunctional monomers in the presence of free-radical initiating species follow radical chain polymerization in which the reaction rate is given by:

$$R_p = \frac{k_p}{k_t^{0.5}}[M](\varphi_i I_{abs})^{0.5} \quad 3.8$$

Equation 3.8 shows the dependence of polymerization rate, R_p, on the rate constant for propagation, k_p, the square root of the rate constant for termination, k_t, the monomer mixture concentration [M], the initiation quantum yield φ_i of the photoinitiator, and the absorbed intensity I_{abs} in the sample. Thus,

$$R_p \alpha \frac{k_p}{k_t^{0.5}} \quad 3.9$$

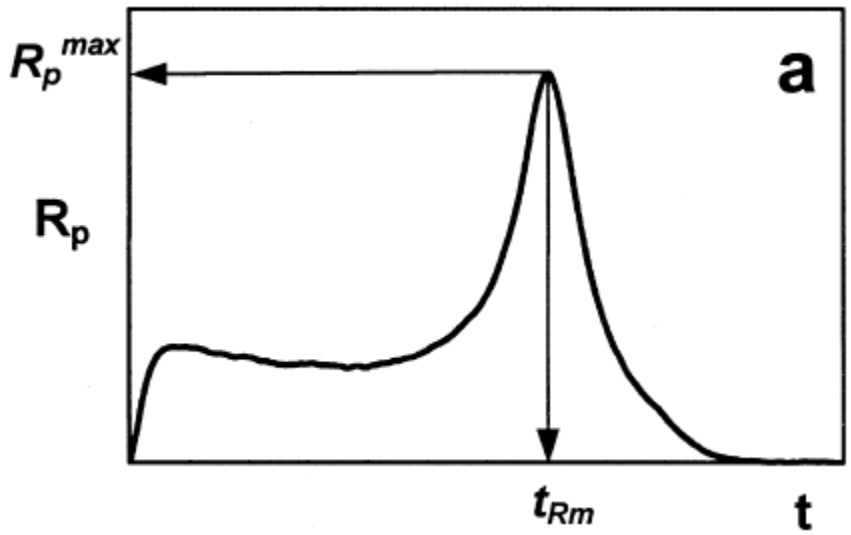

Figure 3.2 Polymerization rate as a function of irradiation time.

It has been found that the polymerization reaction of multimethacrylates and multiacrylates is diffusion-controlled [24]. A few seconds after irradiation, the auto-accelerative gel effect is seen in which the segmental movement of radicals is restricted and termination becomes diffusion-controlled, leading to an increase in the polymerization rate. During this stage of reaction, k_t in Eq. (3.8) decreases and results in a dramatic increase in R_p. Continuing the reaction, the system becomes more viscous and

restricted so that the propagation reaction also becomes diffusion-controlled. At this stage, k_p in Eq. (3.8) also decreases leading to a fall in the polymerization rate. This decline in the rate is called auto-deceleration or the glass effect, the latter relating to the onset of vitrification.

3.3 Shrinkage Measurement Apparatus

Photopolymerization reaction kinetics can often be monitored in-situ by means of photo differential scanning calorimetry (photo-DSC) and Fourier transform infrared spectroscopy (FTIR). Both these instruments need to be equipped with the UV light pen to initiate the curing reaction in the UV-sensitive ceramic-filled resin composition. In this section, the working principles of each of the above mentioned apparatuses are described in detail.

3.3.1 Photo Differential Scanning Calorimetry (Photo-DSC)

The photo-DSC device which, measures the exothermic heat flow from the free-radical photopolymerizing sample, is a proven method of determining polymerization kinetics. The liquid composition is placed in an aluminum pan and exposed to a UV source. With the acrylate monomer C=C bond breakage as the only heat released during the experiment, the percent conversion of monomer C=C bonds can be calculated from the heat flow values. The photopolymerization rate is determined from the measured heat flow by:

$$R_p = \frac{dH}{dt}\frac{1}{\Delta H_p m} \qquad 3.10$$

Where dH/dt is the heat flow measured by the photo-DSC, m is the mass of the pure monomer in the sample; ΔH_p is the experimentally determined enthalpy of polymerization for the acrylate double bond. The rate calculations represent the fraction of C=C bonds reacting in the sample per unit exposure dose. The percent conversion α is then calculated by summing the exothermic heat flow up to the time t, and dividing by the expected heat of polymerization of the monomer [8] as follows:

$$\alpha_t = \frac{\Delta H_{sample}(t)}{\Delta H_p \times m} \times 100 \qquad 3.11$$

3.3.2 Fourier Transform Infrared Spectroscopy (FTIR)

FTIR spectroscopy is an analytical tool used to determine various chemical species and bonds in a molecule. It is one of the most powerful analytical methods for monitoring UV-initiated curing processes which proceed within a fraction of a second. It has several advantages over other methods such as photo-DSC. The most important limitation of photo-DSC is its long response time. Hence, using photo-DSC it is not possible to monitor polymerization reactions which occur within 10s, [8]. In addition, the photo-DSC method requires knowledge on the theoretical enthalpy of reaction to calculate the conversion of functional groups from the heat release measured. Moreover, the thickness of the layer in the aluminum pan is poorly controlled. In contrast, FTIR spectroscopy allows a rapid and quantitative measurement of the conversion of specific reactive functional groups under varying conditions of light intensity, photoinitiator concentration, coating thickness, etc. which are closely matched to those in technical coating and printing processes than can be done with photo-DSC. It was noted in chapter 2 that FTIR spectroscopy has been successfully used to study the kinetics of

photopolymerization reactions, the dependence on the irradiation conditions, and other experimental parameters such as the reactivity of monomers and the efficiency of photoinitiator systems [13, 25]. In the present study, the performance of photoinitiator species when irradiated with monochromatic UV light and the kinetics of the proceeding ultrafast photopolymerization reaction were studied by FTIR spectroscopy to monitor conversion and polymerization shrinkage. Further, the effect of several physical and chemical factors on the kinetic behavior will be discussed and the extent of shrinkage will be estimated. Figure 3.3 represents FTIR operated in attenuated total reflectance (ATR) mode. The sample is held by a pressure device in contact with a crystal, while the IR beam is made to strike the sample with a set of mirrors. This results in a spectrum which is unique to a specific composition and hence can be regarded as the molecular finger print of the sample, as in no two unique molecular structures would produce same spectra.

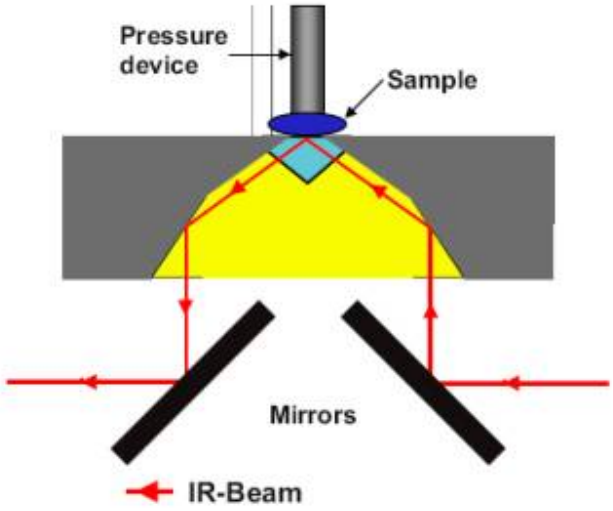

Figure 3.3 FTIR operated in attenuated total reflectance (ATR) mode.

Typical depth of penetration in ATR ranges from 0.5μm to 5μm depending upon wavelength of the IR beam, refractive index of the sample and crystal and angle of incident radiation. During the polymerization of an acrylate monomer, the carbon double bond conversion takes place by means of stretching and twisting [8]. Stretching is sensitive at the 1640-1610 cm^{-1} wavenumbers while twisting is sensitive at 1410 cm^{-1}, as can be seen from the peaks in figure 3.4. The conversion of double bonds during photopolymerization is captured as a function of the exposure time or the energy dose supplied for the reaction. By increasing the exposure time, peak heights are reduced and flatten out indicating the progress of the reaction. In order to quantify the amount by which the carbon double bond peak decreases, comparison with a standard peak which does not change with respect to exposure time is necessary. In other words, it is essential to have an inert or non participating species in the composition. For the acrylate monomer, the carbon oxygen bond (C=O) at 1750 cm^{-1} is taken as the reference peak since it remains constant with time. The degree of conversion α(t) is obtained through Eq. 3.12 and the rate of polymerization can be evaluated by numerically differentiating Eq. 3.12.

$$\alpha(t)=\frac{\left[\frac{Area_{1620}+Area_{1410}}{Area_{1750}}\right]_0-\left[\frac{Area_{1620}+Area_{1410}}{Area_{1750}}\right]_t}{\left[\frac{Area_{1620}+Area_{1410}}{Area_{1750}}\right]_0}X100 \qquad 3.12$$

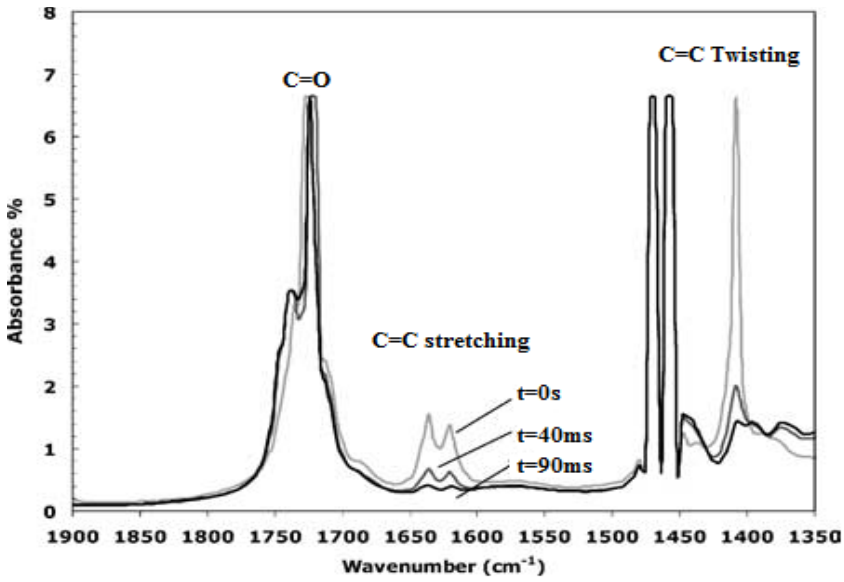

Figure 3.4 FTIR spectrum of acrylate monomer undergoing photopolymerization [8].

3.4 Theoretical Relationship Between Shrinkage and Degree of Conversion

In the polymer science literature it is widely accepted that the dominant cause of shrinkage-strain in acrylates arises from conversion of C=C double bonds, where for each monomer segment of the chain, the larger van der Waals intermolecular spacing is replaced by the smaller intramolecular covalent bond [3, 26]. This results in density changes as the monomer molecules link to form a network of polymer [3]. Thus an exact semi empirical relationship can be derived. Experimentally, the volume change per mole of acrylate groups (C=C) is $\Delta V_{C=C}$ = 22.5 cm^3/mol [27] when acrylate monomer is polymerized. The molar volume of monomer is

$$\frac{M_m}{\rho_m} = \frac{226}{1.01} = 223.76 \text{ cm}^3/\text{mol}, \qquad 3.13$$

where M_m is the molecular weight and ρ_m is the density of the monomer.

Hence the first estimate of volumetric shrinkage strain rate of acrylate monomer is

$$\frac{22.5}{223.76}\text{x}100=10.05\%\,. \tag{3.14}$$

In the more general case of multiacrylates with filler particles, where f is the functionality of the monomer, FL is the filler loading in percentage, the number of functional groups present in volume (V) is

$$\left[\text{f}\times\frac{\text{V}\rho_{\text{m}}}{\text{M}_{\text{m}}}\right]\times\left[1-\frac{\text{FL}}{100}\right] \tag{3.15}$$

The number of functional groups reacted in volume (V) is

$$\alpha(\text{t})\times\left[\text{f}\times\frac{\text{V}\rho_{\text{m}}}{\text{M}_{\text{m}}}\right]\times\left[1-\frac{\text{FL}}{100}\right] \tag{3.16}$$

The percentage relative change in volume (volumetric shrinkage strain) is

$$\frac{\Delta\text{V}}{\text{V}}(\%)=22.5\times\alpha(\text{t})\times\left[\text{f X}\frac{\rho_{\text{m}}}{\text{M}_{\text{m}}}\right]\times\left[1-\frac{\text{FL}}{100}\right]\times100 \tag{3.17}$$

For a mixture of monomers of any functionality,

$$\frac{\Delta\text{V}}{\text{V}}(\%)=22.5\times\alpha(\text{t})\frac{\sum_{\text{i}}(\text{f}_{\text{i}}\chi_{\text{i}})}{\sum_{\text{i}}(\text{M}_{\text{mi}}\chi_{\text{i}})}\rho_{\text{mix}}\times\left[1-\frac{\text{FL}}{100}\right]\times100 \tag{3.18}$$

where f_i is the functionality of monomer (i), χ_i is mole fraction of monomer (i), M_{mi} is molecular mass of monomer (i) and ρ_{mix} is density of the monomer mixture,.

For example, with two monomers, one di-functional (Hexanediol diacrylate, HDDA) and another tetra functional (Ethoxylated penta erythryitol tetra acrylate, EPETA),

$$\frac{\Delta\text{V}}{\text{V}}(\%)=22.5\times\alpha(\text{t})\frac{2\chi_1+4\chi_2}{\text{M}_{\text{m1}}\chi_1+\text{M}_{\text{m2}}\chi_2}\rho_{\text{mix}}\times\left[1-\frac{\text{FL}}{100}\right]\times100 \tag{3.19}$$

Eq 3.17-3.19 embody the expectation that the volumetric shrinkage-strain will be directly proportional to the degree of conversion in the monomer systems. Hence if the conversion diminishes for any reason, the shrinkage strain should also be observed to decrease. Unless significant local porosity is induced within the material bulk, the local shrinkage strain will translate into an observable macroscopic shrinkage-strain.

3.5 Resin Composition and Properties

A typical photopolymerizable material composition for LAMP consists of a mixture of monomers with ceramic particles as filler content and a dispersant to prevent clogging of these ceramic particles. The photoinitiator system is chosen such that it matches with the spectral characteristics of the UV source used for maximal utilization of the free radicals. Absorbers could further be used to alter the cure depths based on the process requirement. The monomers system used in this study is a mixture of HDDA and EPETA in the ratio of 9:1. HDDA is a low volatile, low viscosity monomer, while EPETA is a fast curing monomer. Silica particles with 7μm mean diameter and with 95% of all particles less than 25μm in diameter were chosen as filler particles. The dispersant is Variquat CC59 and it prevents the clogging of the filler particles.

3.5.1 Criteria for Selection of Photoinitiators

Since monomers in the reaction are not capable of absorbing the UV radiation to an adequate extent, it is necessary to add photoinitiators, which do not take part in the photochemical reaction, but are capable of absorbing the irradiated light or UV radiation. The photoinitiators transfer the energy thus absorbed to the monomer mixture, thus

forming active initiator radicals which, in turn, initiate the photopolymerization reaction. Essential criteria for the selection of such initiators depend on the nature of the reactions to be carried out, the relationship of the absorption spectrum of the photoinitiator to the spectral distribution of energy of the available source of radiation, the solubility of the photoinitiator in the reaction mixture, the stability of the reaction system to which the initiator has been added when stored in the dark, and the effect on the end products caused by residues remaining therein of the photoinitiator and/or of the products formed during the photochemical reaction. In particular, the rate of the reaction depends greatly on the photoinitiator used [12]. In this experimental study, two commercially available photoinitiators, Irgacure 184 and Irgacure 819 from Ciba Inc., have been chosen based on the above discussed criteria. The emission spectrum of the high pressure mercury vapor lamp source used in LAMP and the absorption spectrum of IR 184 and IR 819 are shown in figures 3.5, 3.6 and 3.7 respectively. Irgacure 184 exhibits a broad UV absorption spectrum over the 200 to 400 nm range, resulting in an excellent balance of surface and through cure properties. High extinction coefficients of Irgacure 184 at shorter wavelengths (<300nm) result in efficient absorption of UV radiation at the coating's surface. This leads to the formation of a high concentration of photoinitiator radicals at the surface which is sufficient to consume oxygen and still provide excellent surface cure and through cure. Irgacure 819 is also a versatile photoinitiator for radical polymerization of unsaturated resins upon UV light exposure even at very low concentrations. It is especially suited for highly opaque white ceramic formulations and the cure-through is greater than that for Irgacure 184. Further, by adding UV absorbers, the polymerization rate can be slowed down and the cure-through can be controlled as desired.

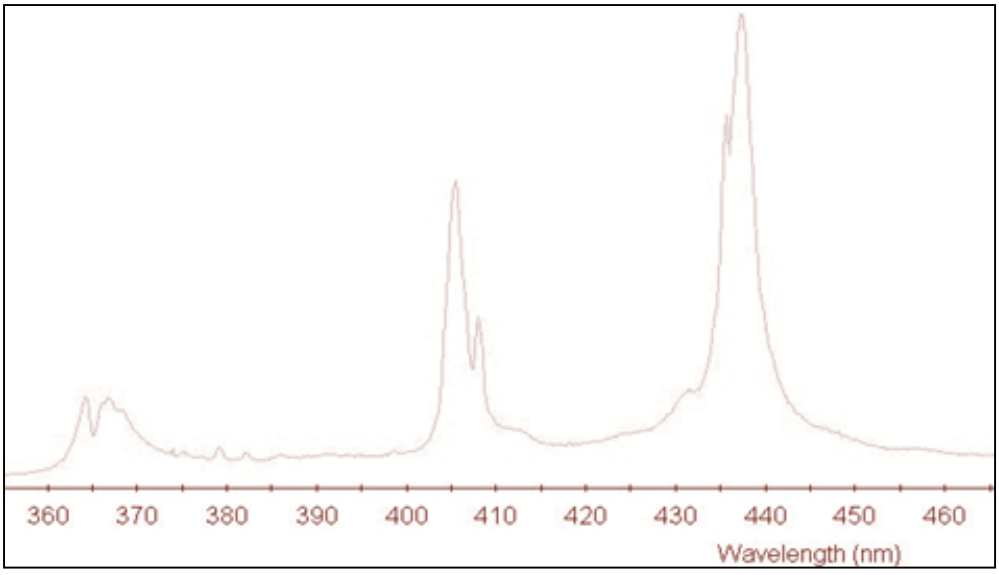

Figure 3.5 Spectrum of high pressure mercury vapor lamp.

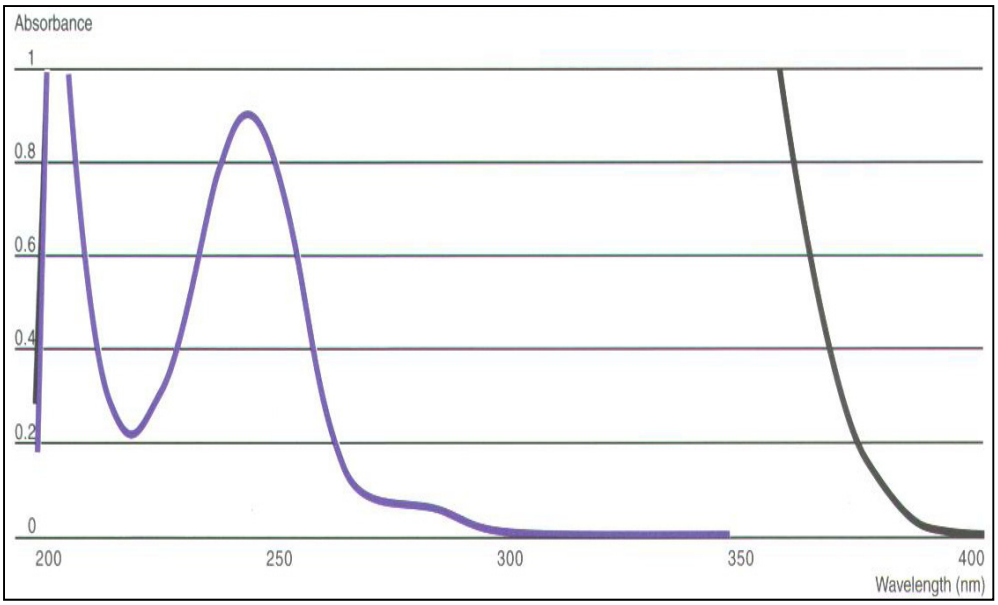

Figure 3.6 Absorption spectrum of IR 184 [28].

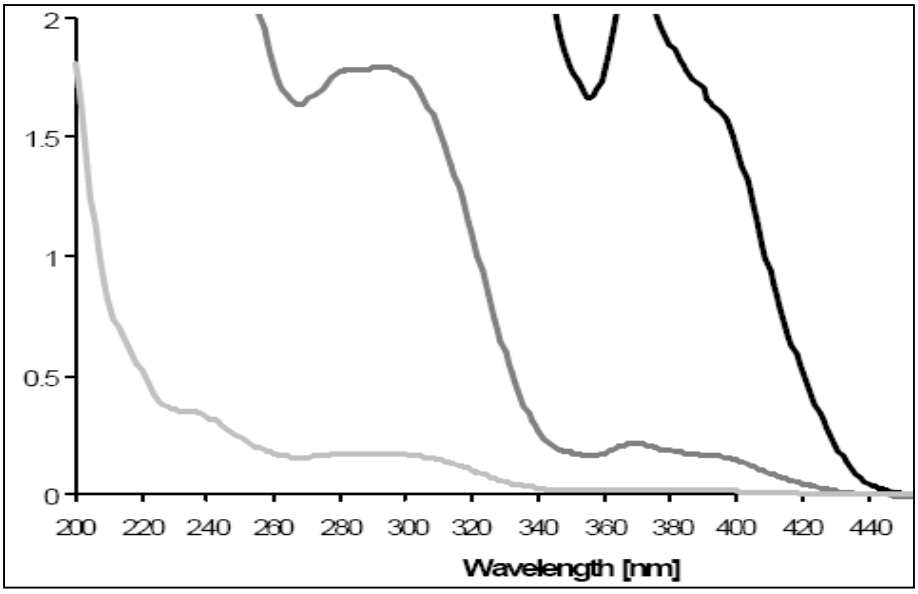

Figure 3.7 Absorption spectrum of IR 819 [28].

3.6 Summary

In this chapter, fundamentals of photopolymerization reaction are discussed along with several experimental techniques available from the literature to determine shrinkage. The details of all the experiments performed were also discussed in the previous sections and the results would be presented in Chapter 4. Photo-DSC and FTIR spectroscopy were discussed in detail outlining their range of applicability and ease of use. Application of FTIR as an effective analytical tool to estimate the degree of conversion in a photopolymerization reaction was established. A semi-empirical relationship between the degree of conversion and the relative volumetric shrinkage strain was discussed. The composition of the ceramic filler-loaded resin is described and the important factors to be considered prior to selection of photoinitiators were enunciated.

CHAPTER 4

RESULTS AND DISCUSSION

In this chapter, the objective of determining the curing kinetics and minimizing the polymerization shrinkage is achieved by systematically investigating the effects of some of the key components of the material system. They are the photoinitiator concentration, the filler loading, and the energy dose or the exposure time. Low exposure time results in poor layer-to-layer bonding while high exposure times lead to print-through, over-curing and side-scattering effects. Very low filler content results in poor mechanical properties and higher conversion leading to increased contraction rates, while very high filler content restricts the mobility of the monomer molecules and hence the conversion. Optimizing these parameters is critical in order to minimize the processing time and shrinkage strain for parts fabricated using LAMP. With these objectives in mind, two sets of experiments were designed. Firstly, the effect of varying photoinitiator concentration was studied by keeping the filler loading percentage constant. Second, the effect of varying filler loading was studied by fixing the photoinitiator concentration at a constant value. Within the first set of experiments with varying photoinitiator concentration, two photoinitiators, Irgacure 184 (IR 184) and Irgacure 189 (IR 819) were chosen and their performances were evaluated. The details are listed in Table 4.1. Starting exposure times were chosen after several trial experiments to determine exposure times necessary for the onset of photopolymerization. The samples thus prepared using the LAMP machine were analyzed using an FTIR spectrometer by taking enough

precautions to prevent further visible light curing. This enabled determination of conversion purely due to photocuring by the UV source in the LAMP machine.

Table 4.1 Experimental parameters.

Set	PI concentration (%)	Exposure time (ms)	Power input (W/cm^2)	Filler Loading (Vol %)
1	0.2-0.6 IR 184 0.6-1.2 IR 819	35-100 20- 40	1.64	60
2	0.43 IR 184	60-85	1.64	10 - 80

4.1 Effect of Varying Photoinitiator Concentration

Increasing the initiator species strongly accelerates the rate of photopolymerization of the monomer mixture, and the maximum polymerization rate is achieved earlier in the reaction. In contrast, the induction period is barely influenced except at the lowest concentration. The polymerization rate R_p in a light-induced reaction depends on: (i) the number of absorbed photons, (ii) the efficiency with which the deposited energy is utilized in the generation of radicals, and (iii) the reactivity of those radicals with the monomer and the growing chain. It can be calculated as follows:

$$R_p = \frac{k_p}{k_t^{0.5}}[M](\varphi_i I_{abs})^{0.5} \qquad 4.1$$

where, k_p and k_t and the rate constants of chain propagation and termination respectively, [M] is the monomer mixture concentration, φ_i is the initiation quantum yield of the

photoinitiator and I_{abs} is the absorbed intensity in the sample [12]. The absorbed intensity is related to the intensity of the incident radiation, I_0, by,

$$I_{abs} = I_0\left[1\text{-}\exp\left(\text{-}2.303A\right)\right] \quad 4.2$$

A is the absorbance of the sample which is given by Beer-Lambert's law as:

$$A = \varepsilon[PI]d \quad 4.3$$

where ε is the molar extinction coefficient at the wavelength of the absorbed light, [PI] is the photoinitiator concentration, and d is the thickness of the sample. Using Eqns. 4.2 and 4.3, the polymerization rate can be expressed as follows:

$$R_p = \frac{k_p}{k_t^{0.5}}[M]\left\{\varphi_i I_0\left[1\text{-}\exp\left(\text{-}2.303\varepsilon[PI]d\right)\right]\right\}^{0.5} \quad 4.4$$

Eq. 4.4 describes a relationship between the polymerization rate and the photoinitiator concentration. However, this relation naturally depends on [M] even when [PI] is the only experimental parameter which is varied.

4.1.1 Varying Irgacure (IR) 184

The effect of the photoinitiator concentration on the conversion and polymerization rate due to irradiation with UV light is shown in figure 4.1 and 4.2 respectively. The minimum energy dose for onset of polymerization (or the minimum exposure time) decreases with increasing IR 184 concentrations, and monomer conversions as high as 85% are achieved for 0.50 weight % of IR 184. In figure 4.2, it can be seen that the maximum polymerization rate $R_{p,max}$ is observed to occur roughly at the same conversion (i.e. about 30%) at all photoinitiator levels studied with the exception of lowest concentration of IR 184 (0.2 wt%) tested. This is in agreement with

the similar observations made by Scherzer [13]. Accordingly, $R_{p,max}$ can be plotted against the square root of the fraction of the absorbed light (figure 4.3). R_p is proportional to $[1-\exp(-2.303\ [PI]d\ )]^{0.5}$ as seen from Eq 4.4, which is again confirmed from figure 4.3 where no significant deviation from linearity is observed at higher photoinitiator concentrations. Thus the slope of the line from figure 4.3 helps in determining the rate constants of the reaction. On the LAMP machine, the maximum conversion with the fastest curing time per layer occurs at approximately 0.43% of the IR 184 concentration, as seen from figure 4.4. However the fastest curing time may not necessarily ensure good layer to layer bonding with minimum shrinkage strain. This is further discussed in section 4.3.

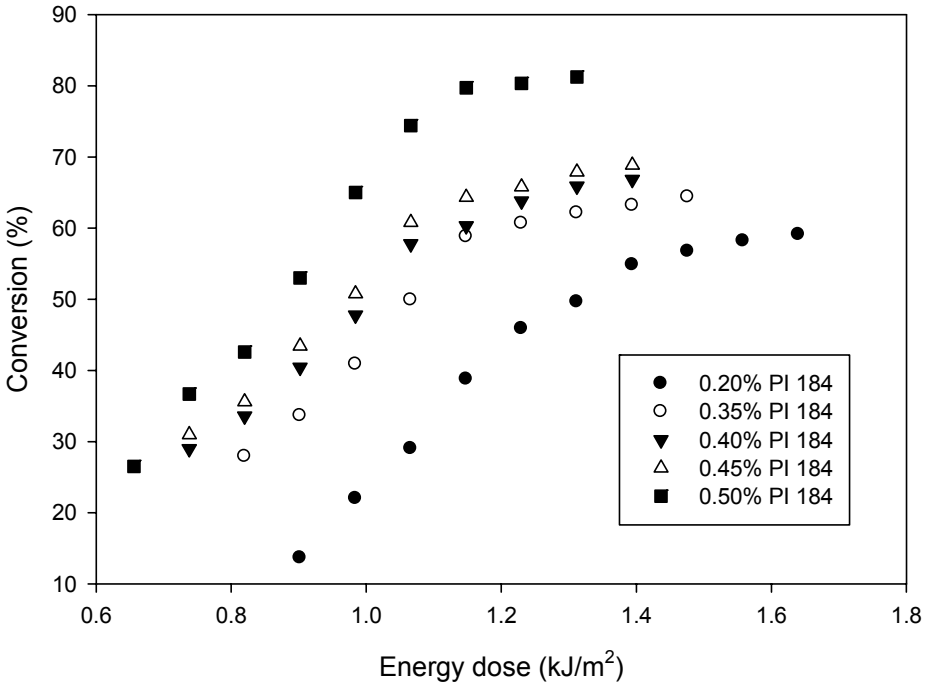

Figure 4.1 Conversion vs. energy dose for varying concentration (wt %) of IR 184.

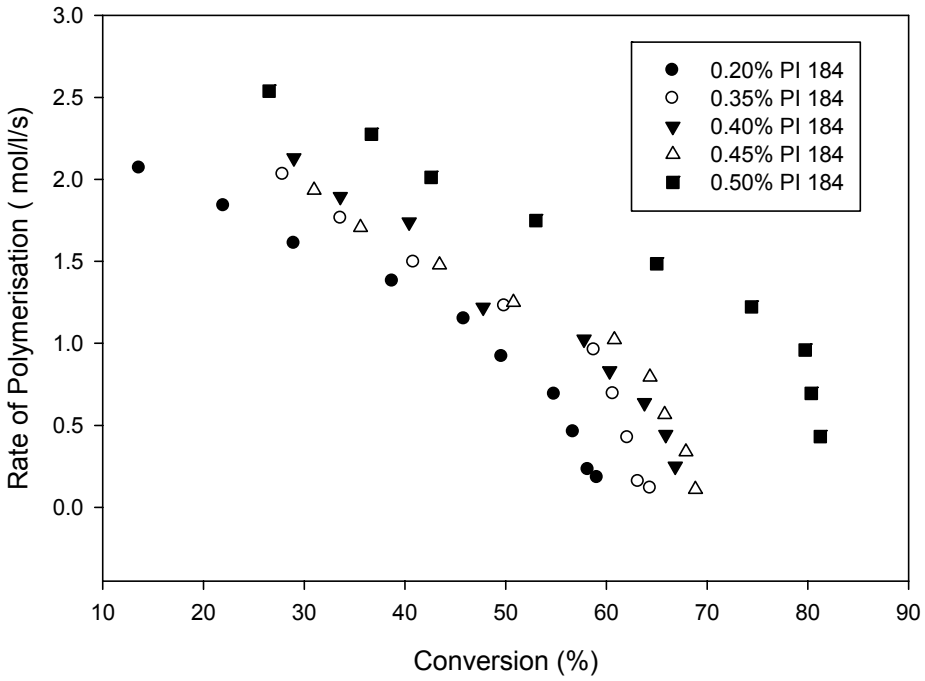

Figure 4.2 Rate of polymerization vs. conversion for varying concentration (wt %) of IR 184.

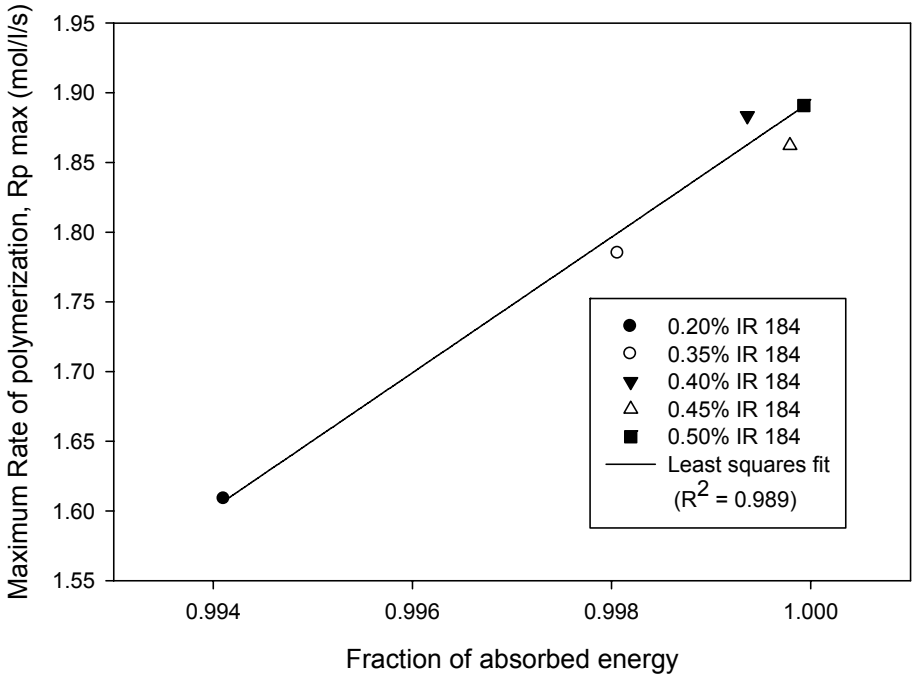

Figure 4.3 Dependence of R_{pmax} on the fraction of absorbed energy for varying concentration (wt %) of IR 184.

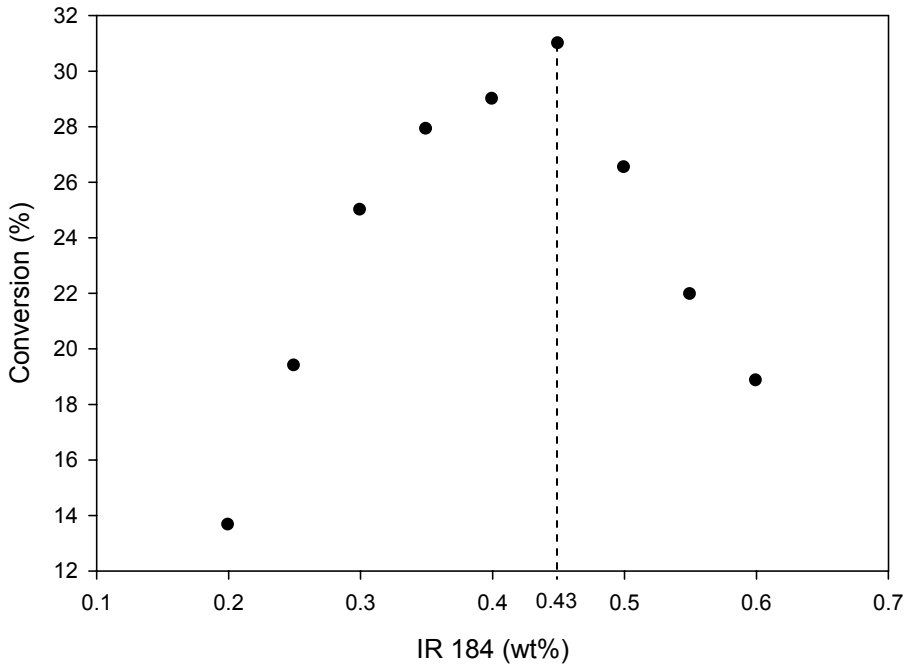

Figure 4.4 Conversion vs. concentration (wt %) of IR 184 for the fastest exposure time on LAMP machine.

4.1.2 Varying Irgacure (IR) 819

Photoinitiator IR 819 is known to exhibit outstanding curing performance at lower concentrations and in the presence of opaque particles [28]. This is an advantage for the LAMP process since overall process time could be drastically reduced with reduced exposure time per layer. Hence, several experiments similar to those conducted with IR 184 were performed and the results are shown in figures 4.5 to 4.8. Even at the lowest tested concentration level of 0.6 wt % of IR 819, a conversion of 40% was obtained with just 20 ms exposure time while a similar conversion using IR 184 required about 50 to 55 ms. However, the shrinkage strain is higher with IR 819 which is further discussed in section 4.3. In figure 4.6, the maximum rate of polymerization R_p occurs within a range of 45-55% conversion as a function of photoinitiator concentration in contrast with

relatively constant 30% conversion seen in the case of IR 184. At the fastest exposure time, conversion increases with increasing concentration of IR 819 as seen in figure 4.7, which was not the case with IR 184. This may be attributed to the extreme sensitivity of IR 819 even at smaller concentration levels. The radicals are consumed at a much faster rate by consuming most of the monomer molecules. In figure 4.8. the least squares linear fit confirms that maximum rate of polymerization $R_{pmax,}$ is proportional to the fraction of absorbed energy as dictated by Eq. 4.4. The slope of this line can be used to determine the rate constants of the polymerization reaction.

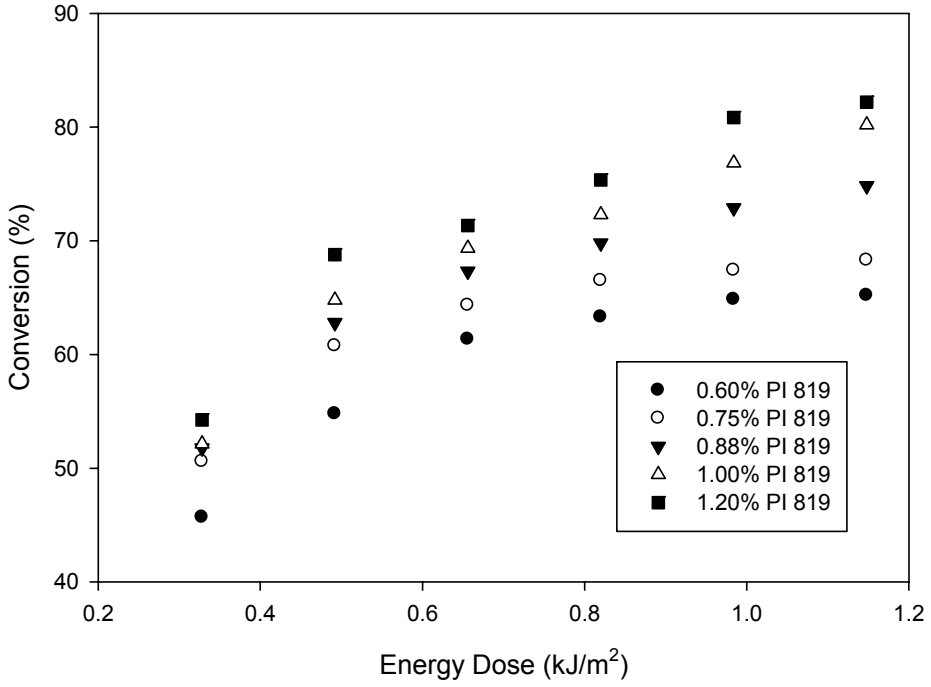

Figure 4.5 Conversion vs. energy dose for varying concentration (wt %) of IR 819.

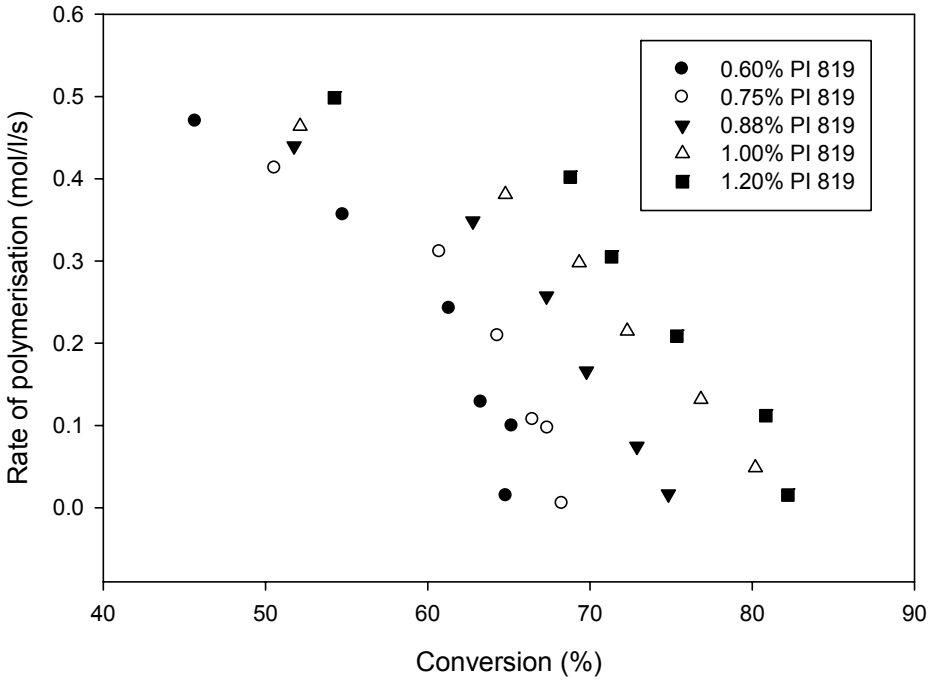

Figure 4.6 Rate of polymerization vs. conversion for varying concentration (wt %) of IR 819.

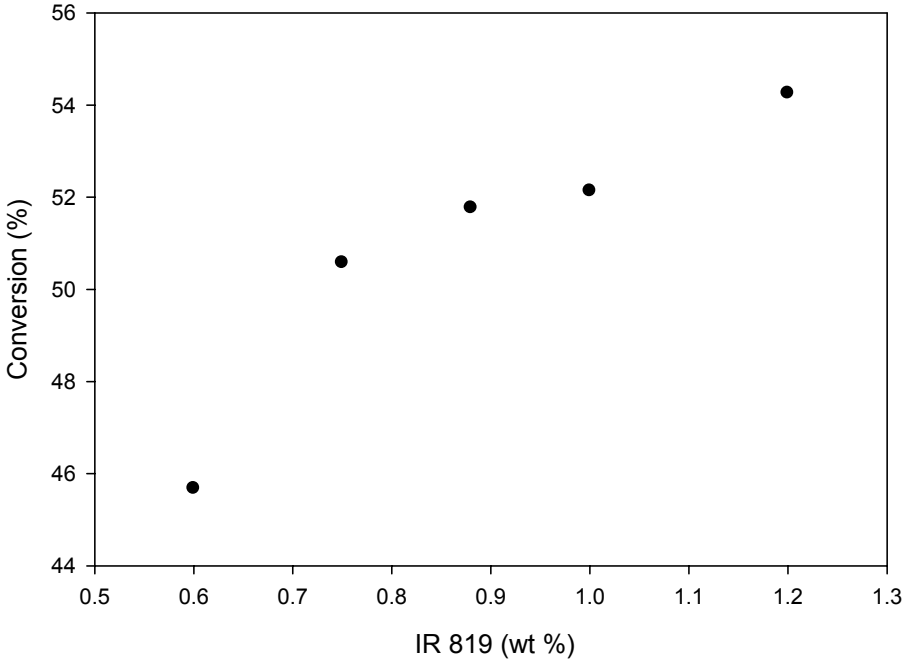

Figure 4.7 Conversion vs. concentration (wt %) of IR 819 for fastest exposure time on LAMP machine.

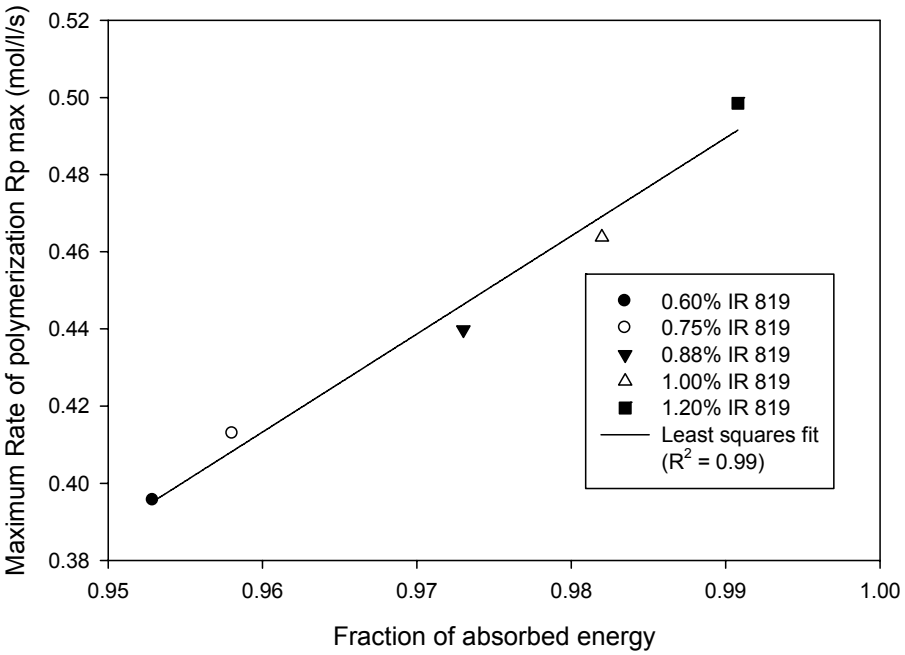

Figure 4.8 Dependence of R_{pmax} on the fraction of absorbed energy for varying concentration (wt %) of IR 819.

4.2 Effect of Varying Filler Loading

In this set of experiments, the volume fraction of the ceramic filler content was varied by keeping the photoinitiator concentration of IR 184 constant at 0.45 weight %. As seen in figure 4.9 and 4.11, the degree of conversion and the rate of polymerization progressively decrease with increasing filler-loading at a given energy dose. This is in agreement with the experimental results of Atai and Watts [2, 7]. At higher filler loading, the mobility of resin-monomers is restricted on the surface of the fillers, leading to a decrease in molecular and radical mobility, resulting in lower conversion. The relative difference in conversions over the range of 10% to 80% filler loading was only about 20 to 25%. Figure 4.12 further illustrates the influence of varying filler loading on conversion at 60ms of exposure time on the LAMP machine. Thus, it seems that the

influence of filler on the conversion and reaction kinetics of the composite is more related to the filler particle-size and surface-area than the filler loading [11]. As in the case of varying photoinitiator concentration, the maximum polymerization rate occurs within the same range of about 40 to 55% conversion, as a function of the filler content (figure 4.10).

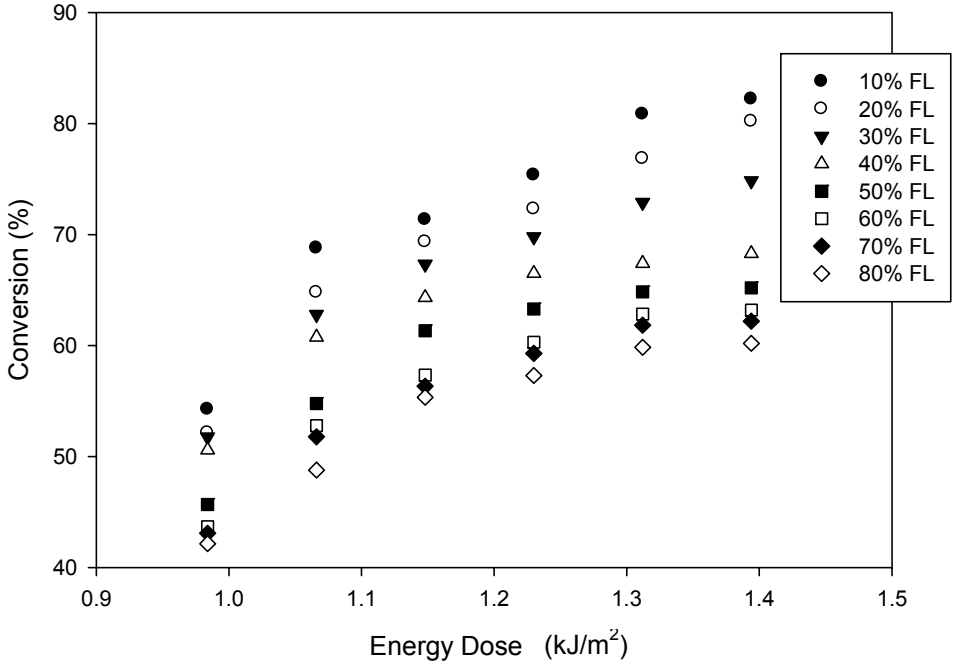

Figure 4.9 Conversion vs. energy dose for varying filler loading (vol %).

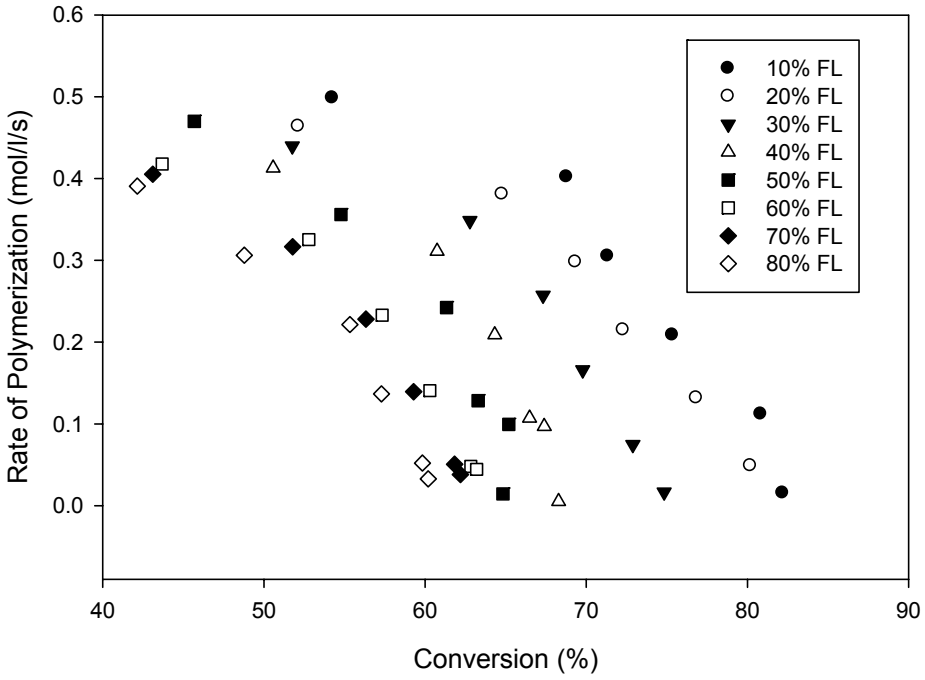

Figure 4.10 Rate of polymerization vs. conversion for varying filler loading (vol %).

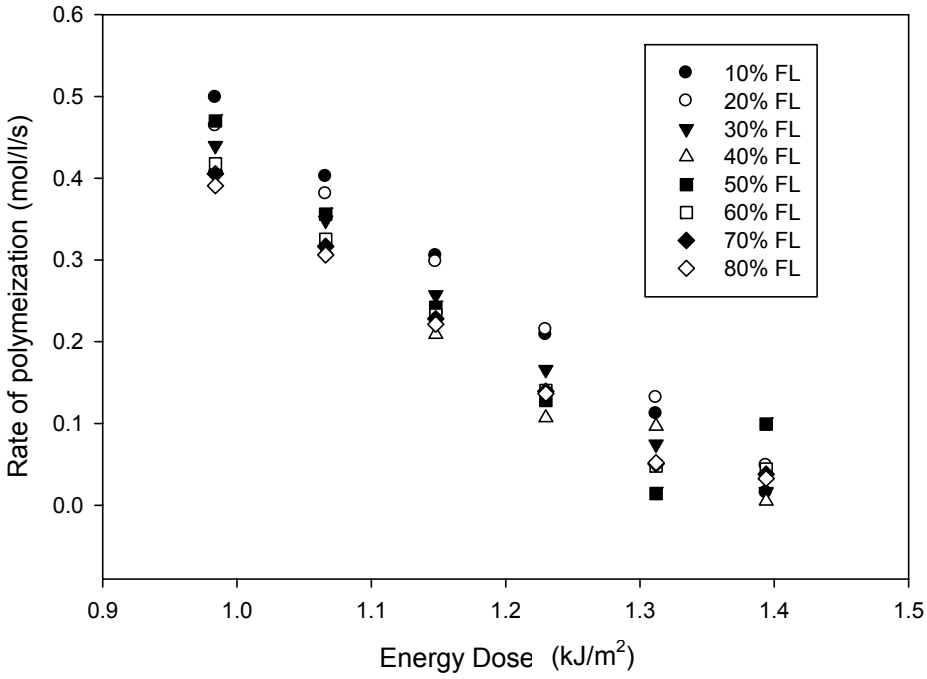

Figure 4.11 Rate of polymerization vs. energy dose for varying filler loading (vol %).

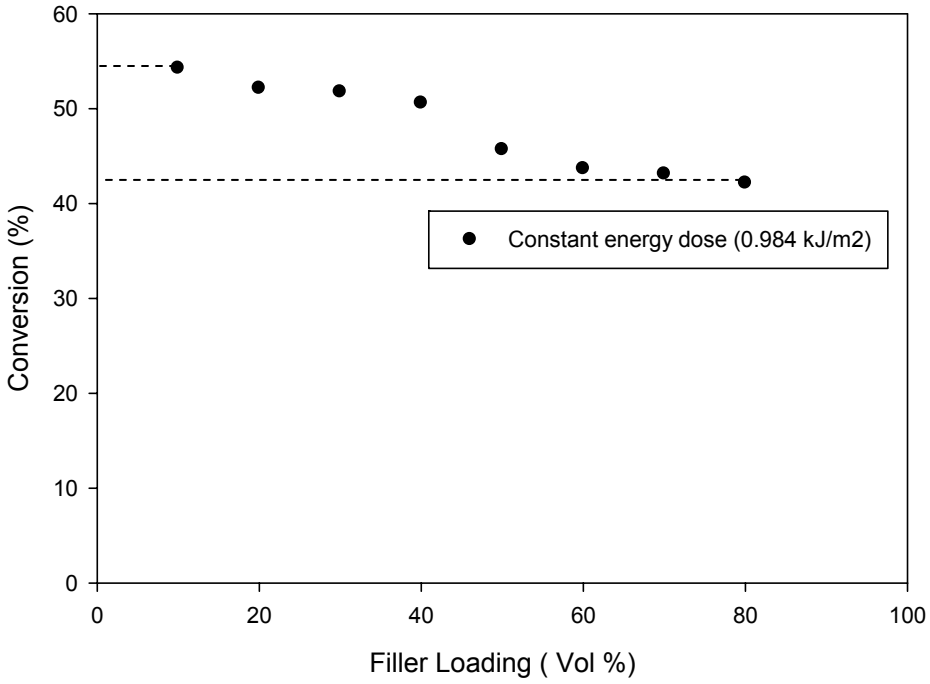

Figure 4.12 Conversion vs. filler loading (vol %) at a constant exposure time of 60ms (0.984kJ/m^2).

4.3 Relative Volumetric Shrinkage Strain

From Eq. 3.19, it can be seen that volumetric shrinkage strain is mainly a function of filler loading and the degree of conversion for a specific mixture of monomers. As discussed in section 3.9, the photocurable material system for LAMP consists of a monomer mixture of HDDA and EPETA in a ratio of 9:1. However, degree of conversion determined from FTIR is a function of photoinitiator concentration, filler loading, and energy dose. Figures 4.13-4.20 help to understand the variation of the volumetric shrinkage strain as a function of all the dependent variables listed above. The volumetric shrinkage strain of the photocurable material system with IR 184 and IR 819 as photoinitiators (with filler loading fixed at 60% by volume) is shown in figures 4.13-4.15

and figures 4.16-4.18, respectively, The volumetric shrinkage strain of the photocurable material system with varying filler content (with photoinitiator IR 184 fixed at 0.43 wt %) is shown in figures 4.19 and figure 4.20.

Figure 4.13 represents a three-dimensional plot of the volumetric shrinkage strain as a function of the energy dose and the degree of conversion for various concentrations (wt %) of IR 184. Figure 4.14 represents projections of various concentration curves of IR 184 onto the plane containing volumetric shrinkage strain and energy dose. It can be seen that the photocurable material system with a higher concentration of IR 184 requires a lower energy dose to achieve a desired degree of conversion. For example, 50% degree of conversion results in approximately 3.972% of volumetric shrinkage strain and to obtain this degree of conversion, the energy dose is decreased from 1.312kJ/m^2 for 0.2% IR 184 to 0.984kJ/m^2 for 0.5% IR 184. Additionally, it can be seen that the minimum energy dose required to start the photopolymerization decreases with increasing concentrations of IR 184. The locus of the minimum energy dose is represented in figure 4.14 labeled “Min ED curve”. The volumetric shrinkage strain along the minimum energy dose curve is seen to increase initially from 1.2% at 0.2% IR 184 and reaches a maximum of 2.5% at 0.45% IR 184 and decreases to approximately 1.8% at 0.5% IR 184. Further, at a constant energy dose, a higher degree of conversion can be obtained by increasing the concentration of IR 184. Thus, at 1kJ/m^2 the degree of conversion increases from approximately 25% for 0.2% IR 184 to 69% for 0.5% IR 184. Figure 4.15 represents projections of all the concentration curves onto the plane formed by the degree of conversion as the abscissa and volumetric shrinkage strain as the ordinate. Equation 3.19 predicts a linear relationship between the volumetric shrinkage strain and the degree

of conversion at a fixed filler loading. As mentioned earlier, for this set of experiments, filler loading is fixed at 60% by volume. Thus, the slope of the line resulting from the intersection of a constant energy dose plane with the plane containing all the concentration curves would be constant. Now, all such lines obtained from the intersection of different constant energy dose planes with the plane containing IR 184 concentration curves collapse onto a single line as seen in figure 4.15.

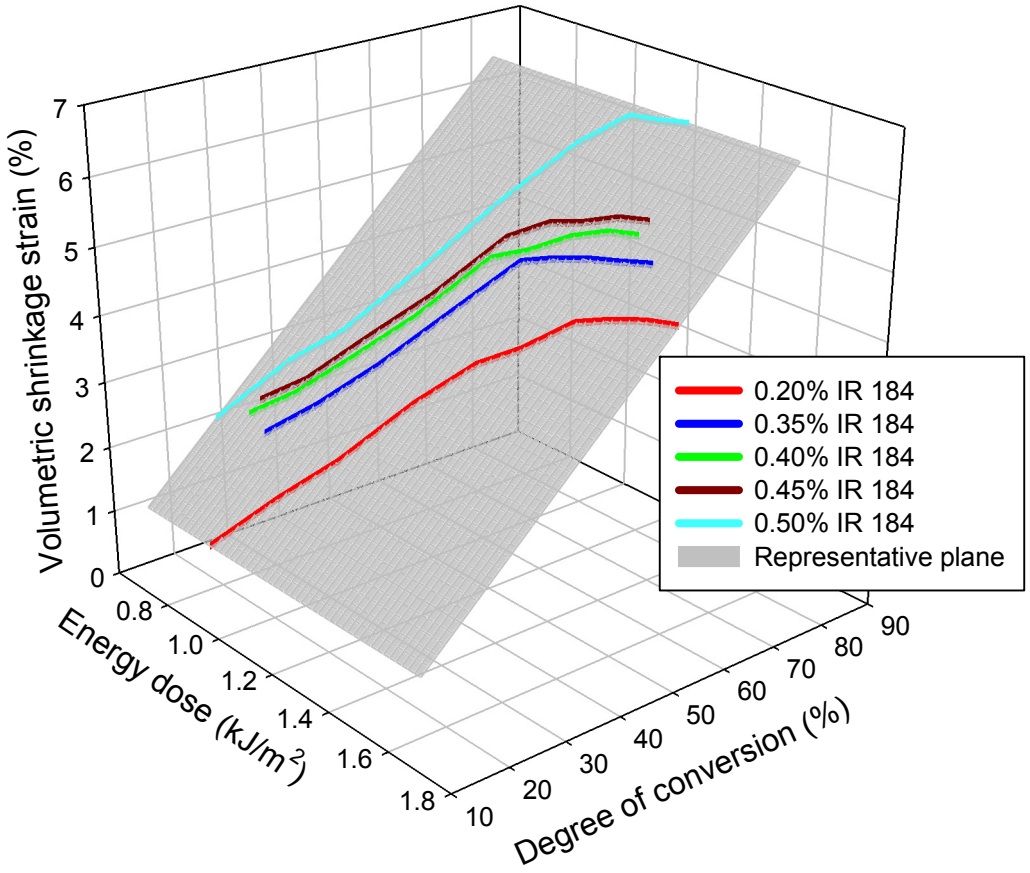

Figure 4.13 Three-dimensional plot of volumetric shrinkage strain as a function of energy dose and degree of conversion for varying concentration (wt %) of IR 184.

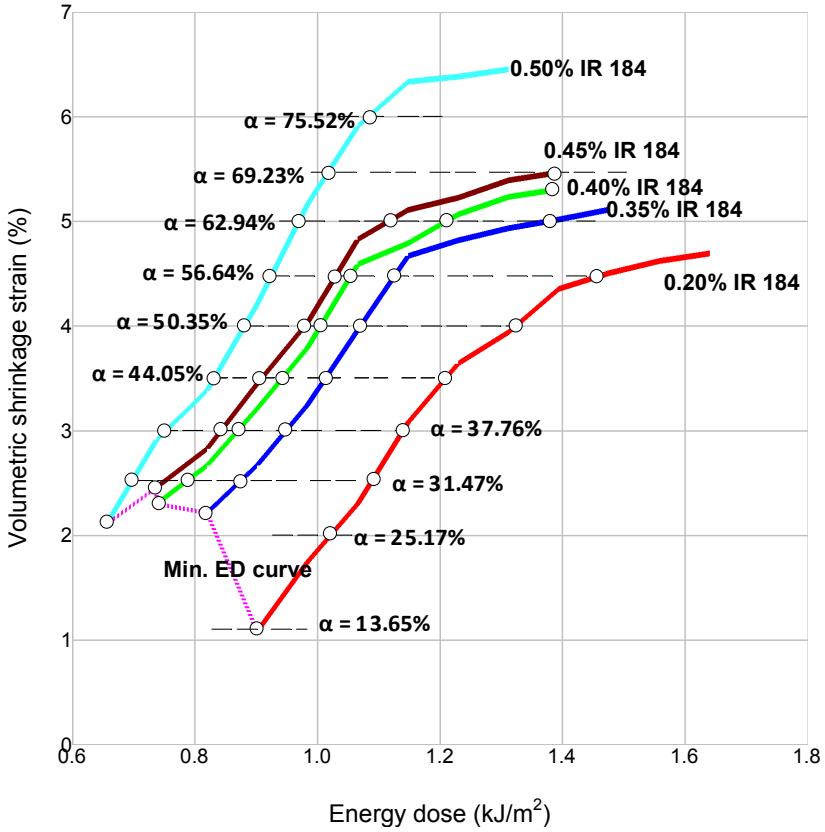

Figure 4.14 Volumetric shrinkage strain vs. energy dose for photocurable material system with 60% filler loading and photoinitiator IR 184. The horizontal dashed lines represent lines of constant conversion levels.

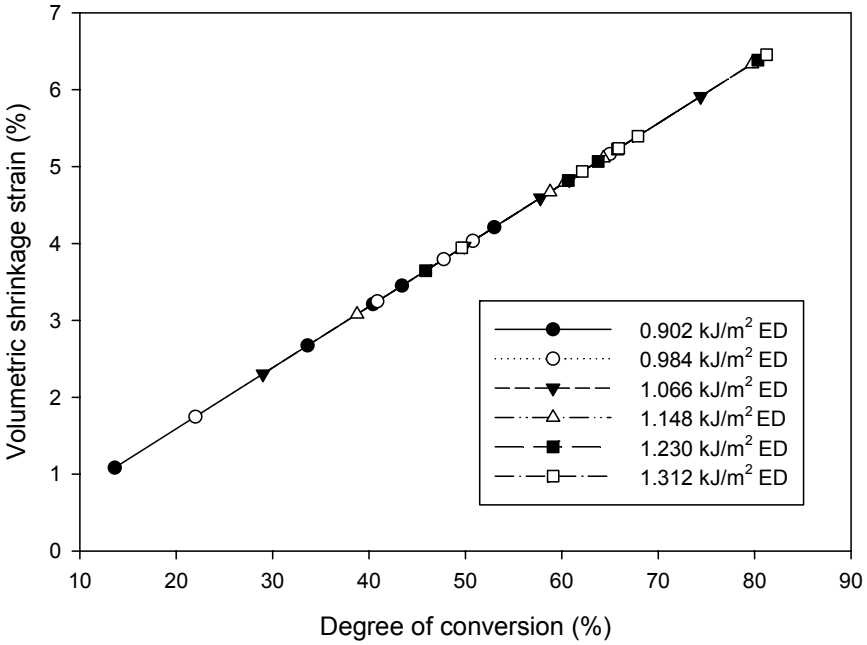

Figure 4.15 Volumetric shrinkage strain vs. degree of conversion for photocurable material system with 60% filler loading and photoinitiator IR 184.

Figure 4.16 represents a three-dimensional plot of the volumetric shrinkage strain as a function of the energy dose and the degree of conversion for various concentrations (wt %) of IR 819. Figure 4.17 represents projections of various concentration curves of IR 819 onto the plane containing volumetric shrinkage strain and energy dose. It can be seen that with an energy dose as little as 0.328kJ/m^2, which also corresponds to the fastest exposure time of 20ms that is achievable on LAMP machine, 50% degree of conversion can be obtained with the lowest tested concentration of 0.6% IR 819. Referring to figure 4.14, the same level of conversion can be obtained by using the highest tested concentration of 0.5% IR 184 with an energy dose of 0.9kJ/m^2, or by using the lowest tested concentration of 0.2% IR 184 with an energy dose of 1.36kJ/m^2 or from a number of intermediate combinations of IR 184 concentration and energy dose values. Since Eq. 3.19 is independent of the type of photoinitiator, 50% conversion using either IR 184 or IR 819 results in 4% volumetric shrinkage strain. It can also be seen from figure 4.17 that the photocurable material system with higher concentration of IR 819 requires lower energy dose to achieve a desired degree of conversion. Further, at a constant energy dose, a higher degree of conversion can be obtained by increasing the concentration of IR 819. For example, at an energy dose of 1kJ/m^2 the degree of conversion increases from approximately 65% for 0.6% IR 819 to 80% for 1.2% IR 819. Similar to figure 4.15, figure 4.18 represents the family of lines obtained from the intersection of different constant energy dose planes with the plane containing IR 819 concentration curves, thus collapsing onto a single line with constant slope.

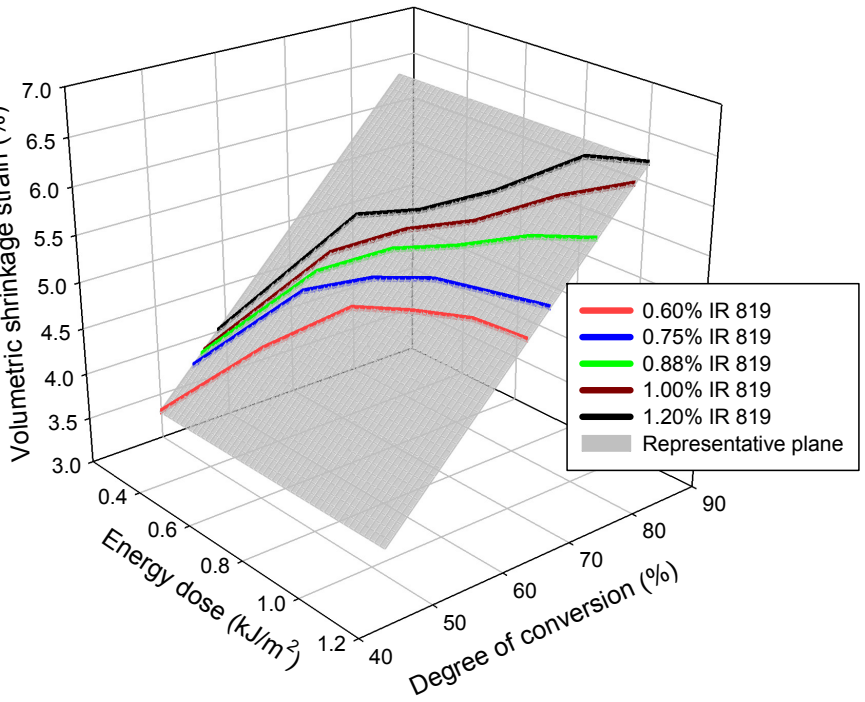

Figure 4.16 Three-dimensional plot of volumetric shrinkage strain as a function of energy dose and degree of conversion for varying concentration (wt %) of IR 819.

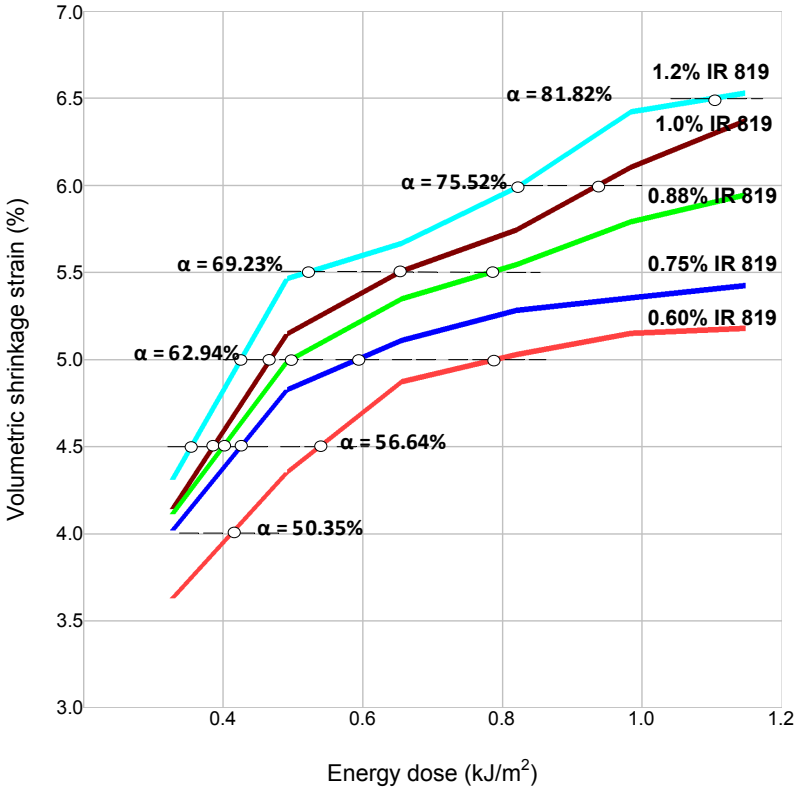

Figure 4.17 Volumetric shrinkage strain vs. energy dose for photocurable material system with 60% filler loading and photoinitiator IR 819. The horizontal dashed lines represent lines of constant conversions levels

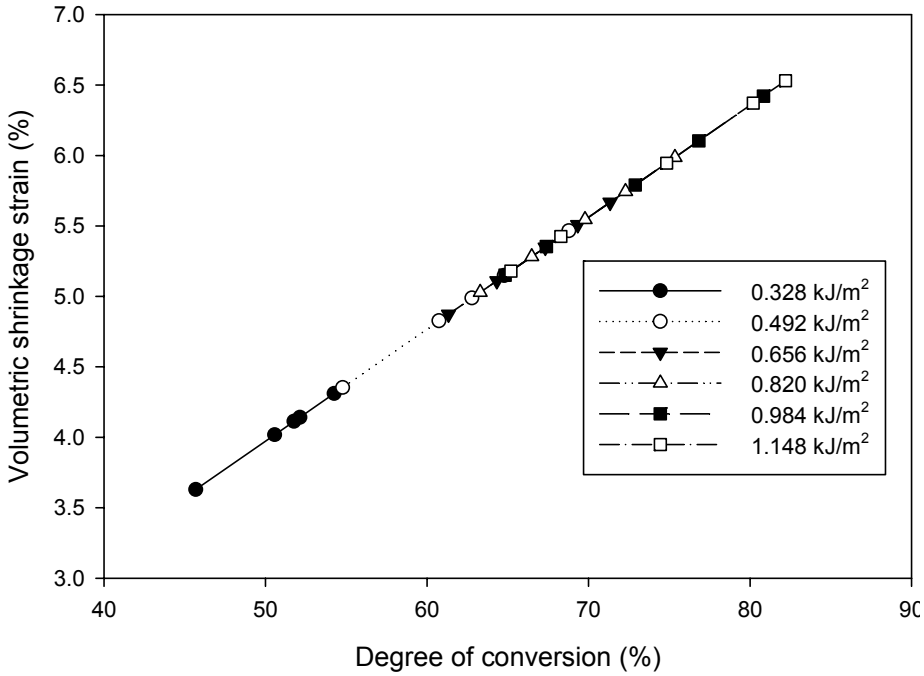

Figure 4.18 Volumetric shrinkage strain vs. energy dose for photocurable material system with 60% filler loading and photoinitiator IR 819.

Figure 4.19 represents three-dimensional plots of the volumetric shrinkage strain as a function of the filler loading and the degree of conversion for varying energy dose. All the space curves in this case do not fall on to the same plane as in figure 4.13 and figure 4.16 since it can be seen from Eq. 3.19 that the volumetric shrinkage strain is both an explicit and implicit function (by means of conversion) of filler loading. Figure 4.20 is obtained by projecting intersection points of several constant filler loading planes with the space curves in figure 4.19 onto a plane containing volumetric shrinkage strain and degree of conversion. Each of the solid or discontinuous lines corresponds to a fixed filler loading plane while each of the colored and segmented lines represents data at a constant energy dose. The slopes of the "constant filler loading" lines increase with decreasing filler content as dictated by Eq. 3.19. From figure 4.20, it can be seen that decreasing the

filler content increases the degree of conversion and volumetric shrinkage strain for a constant energy dose, since the mobility of the monomer molecules is not restricted by the filler particles. For example, an energy dose of 1.148 kJ/m^2 increases the degree of conversion from approximately 55% at 80% filler loading to 70% at 10% filler loading. Further, upon increasing the energy dose from 0.984kJ/m^2 to 1.394kJ/m^2, the relative change in conversion is almost constant for filler loading above 40%, while the relative change in conversion increases with decreasing filler content below 40%. At the 60% filler content which is desired in the photocurable material system for LAMP in order to obtain the required relative density (80-90%) in the final fixed ceramic part, the shrinkage strain is found to vary from 3.5% to 5% over the tested energy dose range of 0.984 to 1.394kJ/m^2.

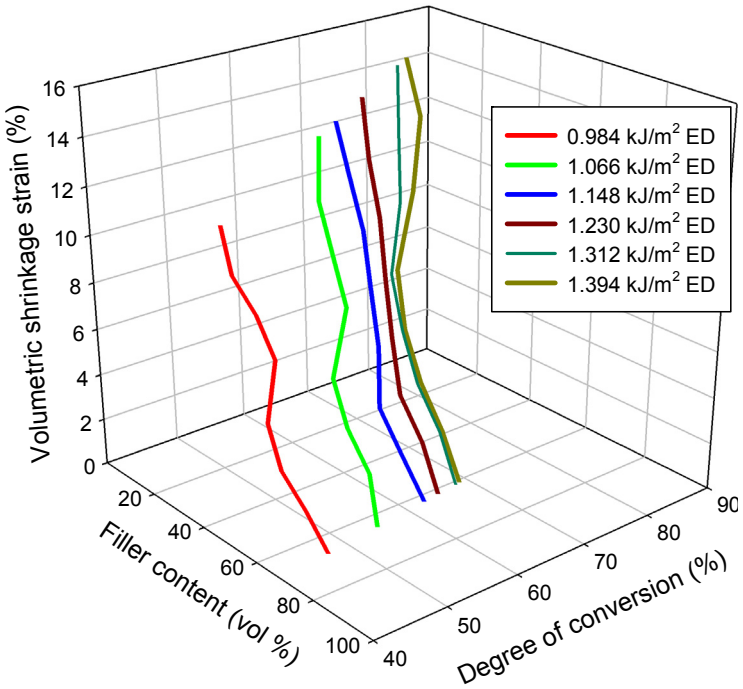

Figure 4.19 Three-dimensional plot of volumetric shrinkage strain as a function of filler loading (vol%) and degree of conversion for varying energy dose and 0.43% of IR 184.

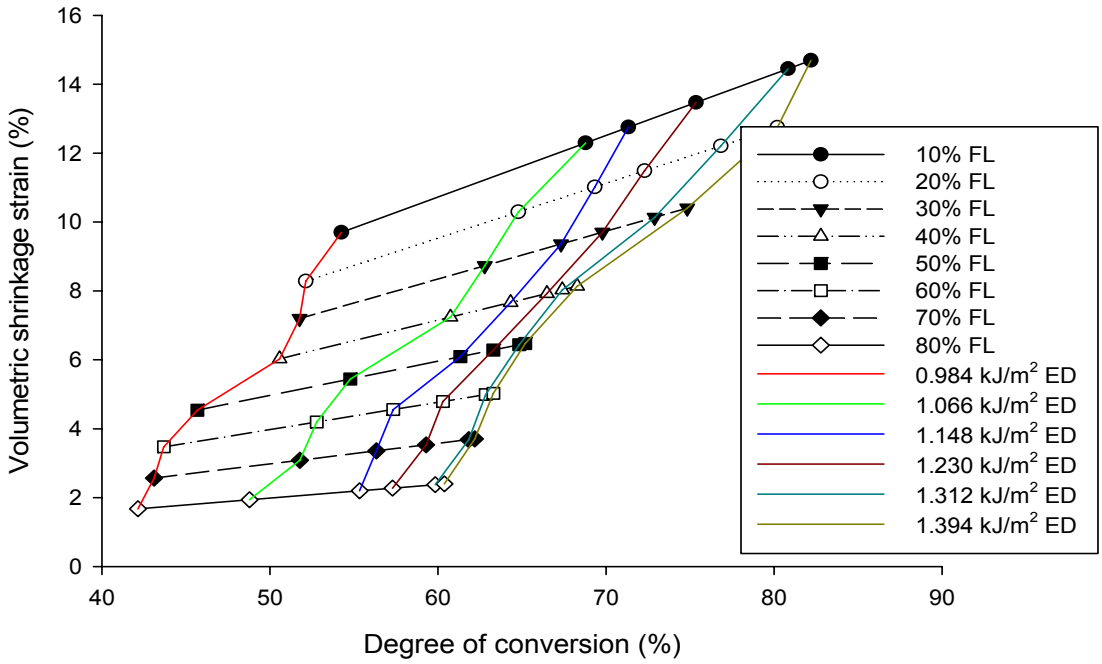

Figure 4.20 Volumetric shrinkage strain vs. degree of conversion for photocurable material system with 0.43% IR 184, varying filler loading (vol %) and energy dose.

It is seen from figure 4.1, 4.5 and 4.9 that higher conversion results from higher photoinitiator concentration and lower filler content. However from figures 4.13 - 4.20, it can be seen that higher conversion results in increased volumetric shrinkage strain in contrast with the objective of minimizing the shrinkage. Hence, it is desired to have high filler content at the expense of decreased conversion. This expense can be compensated by two different means. The first option is to increase the photoinitiator concentration. However, this again leads to the problem of higher shrinkage strain and hence is not desirable. The second option is to increase the filler content at the expense of conversion. This procedure is expected to ensure lower shrinkage strain without compromising on the desired conversion due to the fact that as the parts are being fabricated layer by layer, every layer undergoes additional curing due to print-through which further increases the degree of conversion to a certain extent. This is discussed in more detail in section 4.5.

The shrinkage strain for 0.43% IR 184 at 60% filler loading which is presently used in LAMP is found to vary from approximately 2.5% to 5.5% over a conversion range of 30% to 70% (figure 4.14) while it varies from approximately 4.2% to 6.0% over a conversion range of 56% to 76% with 0.88 % of IR 819. Although the energy dose (exposure time) with IR 819 is much smaller when compared to that with IR 184, it is seen that the shrinkage strain on a layer produced with IR 819 is much higher, which will subsequently worsen with incremental curing due to exposure of layers above. Volumetric shrinkage strain in Eq. 3.19 does not depend on the type of the photoinitiator used. Hence, irrespective of the type of photoinitiator, the photocurable material system can always be designed to obtain a required degree of monomer conversion. At a desired conversion of 50%, the volumetric strain with IR 184 as well as with IR 819 is close to 4%. The performance analysis of photocurable material systems with IR 184 and IR 819 with respect to process time is discussed in next section.

4.4 Shrinkage Strain Comparison Between IR 184 and IR 819

In order to compare the performance of photocurable material systems formulated with IR 184 and IR 819, one composition each with IR 184 (0.43%) and with IR 819 (0.88%) were chosen so as to achieve a 50% monomer conversion and 4% volumetric shrinkage strain in both systems. In figure 4.16 and 4.17, it is clearly seen that IR 819 requires much lower exposure time and yields higher conversion of monomer compared to IR 184. The volumetric shrinkage strain with IR 819 is approximately 5.5% at 50ms of exposure time while it is less than 3% with for IR 184. In addition, a desired conversion of 50% results in 4% shrinkage in both the cases. At this level of conversion and

corresponding shrinkage, the exposure time is slightly more than 20 ms for IR 819, while it is close to 65 ms for IR 184. Thus the major advantage in using IR 819 over IR 184 is that the overall exposure time to achieve the same conversion would be much lower, improving the part build rate. However, it was observed that a 250 layer thick core section of an airfoil part built using IR 819 exhibited much more warpage in comparison with one built using IR 184, suggesting that the extent of internal stress build up is much higher in the parts built using IR 819. This warranted further studies to investigate the print-through due to incremental curing in the layers and is discussed in more detail in the next section.

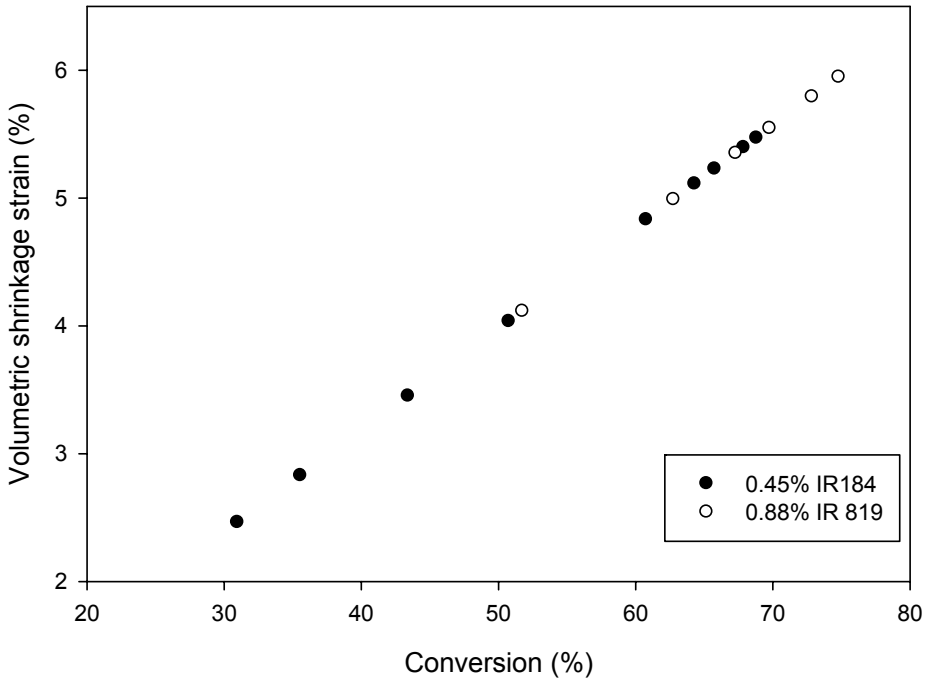

Figure 4.21 Shrinkage strain vs. conversion for IR 184 and IR 819.

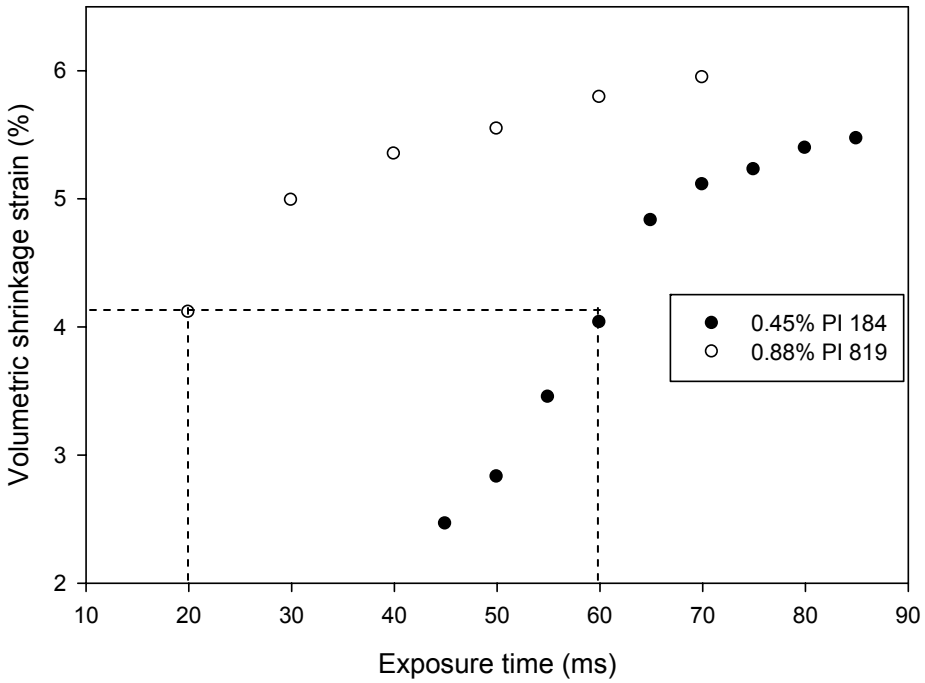

Figure 4.22 Shrinkage strain vs. exposure time for IR 184 and IR 819.

4.5 Print-Through Mediated Incremental Curing

Except for the topmost layer of a built part and for topmost layers of free-standing features, all the layers in a part built through the LAMP process are incrementally cured as subsequent layers above them are being exposed. Print-through results in good layer-to-layer bonding by means of additional curing if it can be restricted to two times the layer thickness. However, additional curing due to light penetration at the bottom layer from several layers above results in accumulation of internal stresses and warping of the fabricated part. Hence, it is desirable to determine the extent to which a particular layer is being cured additionally due to the print-through phenomenon. As shown in figure 4.18, several parts were fabricated with 100 μm thick layers, while print-through is desired to be not more than two layers deep. Experiments were conducted using resin compositions

with varying photoinitiator concentrations to determine the change in conversion as subsequent layers were swept and exposed from above. The bottom layer of each of the samples fabricated with different number of layers above the bottom layer was analyzed using FTIR. The results are shown in figure 4.24.

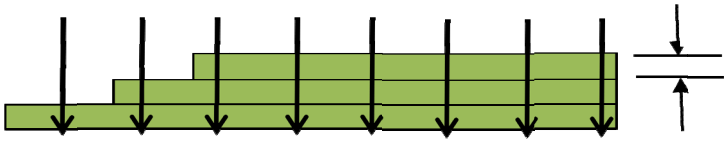

Figure 4.23 Print-through mediated incremental curing at the bottom layer due to exposures of layers above it.

It can be seen from figure 4.24 that with IR 819, the conversion at the bottom layer continuously increases up to approximately 7 exposed layers above, while it is much lower between 2 and 4 exposed layers above for compositions with IR 184. Higher concentrations of photoinitiators in general leads to greater conversion as seen from the previous sections. However, the potential to additionally cure the layers underneath is lower due to the lack of monomer molecules. With 0.69% IR 184, the conversion curve flattens out after two exposures while additional curing is continued until four exposures for 0.43% of IR 184. Also the non-uniformity in the conversion as a result of UV light penetration is much lower in the case of IR 819 as compared to IR 184. This is also an indicative of the deeper curing capability of IR 819. Since the absorption coefficient of IR 184 is much greater than IR 819, an exponential decrease in absorbance results in lower UV light penetration with IR 184 in comparison with IR 819.

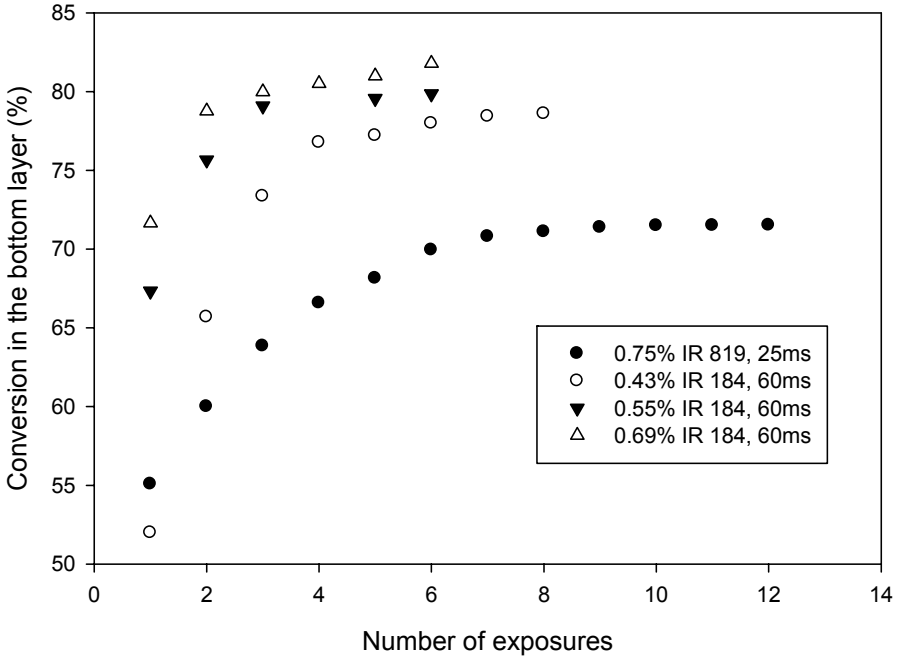

Figure 4.24 Conversion in the bottom layer vs. number of exposures above the bottom layer.

4.6 Summary

Photoinitiators IR 184 and IR 819 were tested systematically over a wide range of concentrations and exposure times. The corresponding kinetic parameters along with the shrinkage strain curves have been obtained. Conversion values reported in the plots are the average of 2 trials, although the UV beam striking the resin surface is uniform throughout the exposure region. These curves could be used as long as the spectral characteristics of the UV source in the LAMP machine remain the same. The choices of photoinitiators have been purely based on their applicability range recommended by CIBA in the specification sheets provided by them [28]. The photoinitiators were chosen by matching their energy absorbing ability with the radiation spectrum emitted by the UV source in the LAMP machine. By using similar procedure, monomer conversions can be

monitored over several different layers as the part is fabricated layer by layer and can be used to determine the cumulative shrinkage strain. This data when used along with the slicing algorithms can accommodate for the shrinkage strain resulting in closer conformation to the desired geometry.

CHAPTER 5

SUMMARY and CONCLUSIONS

In chapter 1, several tasks associated with direct digital manufacturing of airfoils for casting turbine blades were introduced. The work presented in this thesis plays a vital role from the process planning perspective and provides guidelines for determining curing kinetics and volumetric shrinkage in a photocurable material system with IR 184 or IR 819 as photoinitiators without the need for extensive experiments in order to determine the optimum operating parameters. Chapter 2 provides an extensive literature review on the work that has been previously accomplished. Research gaps relevant to the LAMP process were identified. FTIR and photo-DSC measurement techniques were discussed extensively in chapter 3, while FTIR was established as an efficient tool to monitor the photochemical reaction and to estimate the associated degree of conversion and volumetric shrinkage. A semi-empirical relation between the degree of conversion and the volumetric shrinkage as a consequence of the photopolymerization reaction was discussed. The form of this equation depends on the monomer type and monomer mixture ratio which was kept constant with HDDA and EPETA in the ratio of 9: 1.

5.1 Contributions

From the literature review it was seen that majority of the photopolymerization reactions were carried out with pure monomers and characterized using photo-DSC and FTIR. Curing was performed using a UV light pen unlike in LAMP. Wu [8], explored the possibility of using FTIR over photo-DSC for ceramic compositions. The filler used was alumina particles and the experiments were designed only for comparing FTIR with

photo-DSC. In this thesis, experiments have been designed such that the results can serve as reference for LAMP process planning. First estimates of curing kinetic parameters and volumetric shrinkage strain for any composition covered within the range of 0.2 wt % to 0.50 wt % IR 184, 0.6 wt % to 1.2 wt % IR 819 with 60 vol % of silica particles as filler content and 10 vol % to 80 vol % filler content with 0.45 wt % IR 184, can be obtained quickly by referring to the plots in chapter 4. An investigation of print-through mediated incremental curing effects discussed in section 4.5, helps in adjusting the resin sensitivity depending on the layer thickness desired, with the objective of preventing over-curing and unacceptable accumulation of internal stresses. Although significantly decreased the curing times were seen with photoinitiator IR 819, the print-through and hence the accumulation of shrinkage strain was found to be extremely high in comparison with IR 184.

5.2 Future Work

Due to the continuous changes in the material system in order to improve the quality of final part, systems with several other photoinitiators may be designed and similar sets of experiments as those presented in this thesis will need to be performed. Simulations of the LAMP process to determine the curing parameters would be extremely useful from which conversion for a given material system based on applied energy dose could be determined. This would eliminate the need for FTIR to determine volumetric shrinkage strain and could serve as a process planning module for the LAMP machine. Using FTIR, the conversion can be obtained for only one layer at a time and moreover determining conversion in the layers along the part may require complicated bitmap patterns and exposure techniques. This can be avoided by placing strain gauges along the

part as it is being fabricated layer by layer. The data obtained from strain gauges at different heights of the part can be recorded and analyzed to estimate the cumulative shrinkage strain due to photopolymerization reaction. Oxygen inhibition has been found from the literature to play a role in affecting the surface cure [25]. This effect was not seen significantly in LAMP since the energy density of the UV source in LAMP is extremely high (1.64W/cm^2). However, it would be useful to know the extent to which surface cure is affected due to oxygen inhibition. A mixture of two photoinitiators with absorption bands at two different wavelengths is known to provide more uniform conversion along the penetration depth [27]. A strong absorption band gives high intensity at the surface, while a weak absorption band is less affected by penetration and provides more uniform intensity as a function of penetration, thereby reducing the stress build up. However this needs to be confirmed with further experiments.

REFERENCES

1. Smart R.F, B.P.R., *Investment Casting (Materials Science)*. 1995: Maney Materials Science (July 1, 1995).
2. Atai, M. and D.C. Watts, *A new kinetic model for the photopolymerization shrinkage-strain of dental composites and resin-monomers.* Dental Materials, 2006. **22**(8): p. 785-791.
3. Watts, D.C., *Reaction kinetics and mechanics in photo-polymerised networks.* Dental Materials, 2005. **21**(1): p. 27-35.
4. Watts, D.C. and A.A. Hindi, *Intrinsic 'soft-start' polymerisation shrinkage-kinetics in an acrylate-based resin-composite.* Dental Materials, 1999. **15**(1): p. 39-45.
5. Watts, D.C. and A.J. Cash, *Kinetic measurements of photo-polymerization contraction in resins and composites.* Measurement Science & Technology, 1991. **2**(8): p. 788-794.
6. Gao, H. and J. Nie, *Temperature effect on UV-photopolymerization of 1, 6-hexanediol diacrylate.* Fushe Yanjiu yu Fushe Gongyi Xuebao/Journal of Radiation Research and Radiation Processing, 2006. **24**(5): p. 289-292.
7. Alvarez-Gayosso, C., et al., *Calculation of contraction rates due to shrinkage in light-cured composites.* Dental Materials, 2004. **20**(3): p. 228-235.
8. Wu, K.C. and J.W. Halloran, *Photopolymerization monitoring of ceramic stereolithography resins by FTIR methods.* Journal of Materials Science, 2005. **40**(1): p. 71-76.

9. Petrovic, L.M. and T.M. Atanackovic, *A model for shrinkage strain in photo polymerization of dental composites.* Dental Materials, 2008. **24**(4): p. 556-560.

10. Momani, S., Z. Odibat, and V.S. Erturk, *Generalized differential transform method for solving a space- and time-fractional diffusion-wave equation.* Physics Letters A, 2007. **370**(5-6): p. 379-387.

11. Atai, M., D.C. Watts, and Z. Atai, *Shrinkage strain-rates of dental resin-monomer and composite systems.* Biomaterials, 2005. **26**(24): p. 5015-5020.

12. Scherzer, T. and U. Decker, *Kinetic investigations on the UV-induced photopolymerization of a diacrylate by time-resolved FTIR spectroscopy: the influence of photoinitiator concentration, light intensity and temperature.* Radiation Physics and Chemistry, 1999. **55**(5-6): p. 615-619.

13. Scherzer, T. and U. Decker, *Real-time FTIR-ATR spectroscopy to study the kinetics of ultrafast photopolymerization reactions induced by monochromatic UV light.* Vibrational Spectroscopy, 1999. **19**(2): p. 385-398.

14. Lu, B., et al., *Reducing volume shrinkage by low-temperature photopolymerization.* Journal of Applied Polymer Science, 2007. **104**(2): p. 1126-1130.

15. Chung, C.M., et al., *Development of a new photocurable composite resin with reduced curing shrinkage.* Dental Materials, 2002. **18**(2): p. 174-178.

16. Khudyakov, I.V., et al., *Kinetics of Photopolymerization of Acrylates with Functionality of 1â¨'6.* Industrial & Engineering Chemistry Research, 1999. **38**(9): p. 3353-3359.

17. Ferracane, J.L., *Developing a more complete understanding of stresses produced in dental composites during polymerization.* Dental Materials, 2005. **21**(1): p. 36-42.

18. Koplin, C., R. Jaeger, and P. Hahn, *Kinetic model for the coupled volumetric and thermal behavior of dental composites.* Dental Materials, 2008. **24**(8): p. 1017-1024.

19. Pereira, S.G., N. Reis, and T.G. Nunes, *Spatially resolved studies on the photopolymerization of dimethacrylate monomers.* Polymer, 2005. **46**(19 SPEC ISS): p. 8034-8044.

20. Condon, J.R. and J.L. Ferracane, *Reduced polymerization stress through non-bonded nanofiller particles.* Biomaterials, 2002. **23**(18): p. 3807-3815.

21. Goodner, M.D. and C.N. Bowman, *Development of a comprehensive free radical photopolymerization model incorporating heat and mass transfer effects in thick films.* Chemical Engineering Science, 2002. **57**(5): p. 887-900.

22. Atanackovic, T.M., S. Pilipovic, and D. Zorica, *A diffusion wave equation with two fractional derivatives of different order.* Journal of Physics A: Mathematical and Theoretical, 2007(20): p. 5319.

23. Hoyle, C.E., et al., *Photopolymerization of 1,6-hexanediol diacrylate with deoxybenzoin as photoinitiator.* Polymer, 1988. **29**(11): p. 2033-2040.

24. Lee, J.H., R.K. Prud'homme, and I.A. Aksay, *Cure depth in photopolymerization: Experiments and theory.* Journal of Materials Research, 2001. **16**(12): p. 3536-3544.

25. Scherzer, T., *Depth profiling of the conversion during the photopolymerization of acrylates using real-time FTIR-ATR spectroscopy.* Vibrational Spectroscopy, 2002. **29**(1-2): p. 139-145.

26. Hofmann, N., et al., *The influence of plasma arc vs. halogen standard or soft-start irradiation on polymerization shrinkage kinetics of polymer matrix composites.* Journal of Dentistry, 2003. **31**(6): p. 383-393.

27. Silikas, N., A. Al-Kheraif, and D.C. Watts, *Influence of P/L ratio and peroxide/amine concentrations on shrinkage-strain kinetics during setting of PMMA/MMA biomaterial formulations.* Biomaterials, 2005. **26**(2): p. 197-204.

28. *Ciba® IRGACURE® Photoinitiator.* Ciba Specialty Chemicals, Coating Effects Segment, (30.8.2001.Basle).